
Theses and Dissertations

Spring 2015

Optimization-based dynamic simulation of human jogging motion

Kaustubh Anil Patwardhan
University of Iowa

Follow this and additional works at: <https://ir.uiowa.edu/etd>



Part of the [Biomedical Engineering and Bioengineering Commons](#)

Copyright 2015 Kaustubh Anil Patwardhan

This thesis is available at Iowa Research Online: <https://ir.uiowa.edu/etd/1722>

Recommended Citation

Patwardhan, Kaustubh Anil. "Optimization-based dynamic simulation of human jogging motion." MS (Master of Science) thesis, University of Iowa, 2015.
<https://doi.org/10.17077/etd.zprz4ja>

Follow this and additional works at: <https://ir.uiowa.edu/etd>



Part of the [Biomedical Engineering and Bioengineering Commons](#)

OPTIMIZATION-BASED DYNAMIC SIMULATION OF HUMAN JOGGING
MOTION

by

Kaustubh Anil Patwardhan

A thesis submitted in partial fulfillment
of the requirements for the Master of Science
degree in Biomedical Engineering in the
Graduate College of
The University of Iowa

May 2015

Thesis Supervisor: Professor Karim Abdel-Malek
Adjunct Associate Professor Rajankumar Bhatt

Copyright by

KAUSTUBH ANIL PATWARDHAN

2015

All Rights Reserved

Graduate College
The University of Iowa
Iowa City, Iowa

CERTIFICATE OF APPROVAL

MASTER'S THESIS

This is to certify that the Master's thesis of

Kaustubh Anil Patwardhan

has been approved by the Examining Committee for
the thesis requirement for the Master of Science degree
in Biomedical Engineering at the May 2015 graduation.

Thesis Committee:

Karim Abdel-Malek, Thesis Supervisor

Rajankumar Bhatt, Thesis Supervisor

Jasbir Arora

Timothy Marler

Salam Rahmatalla

ACKNOWLEDGEMENTS

First and foremost, I would like to express profound gratitude to my academic advisor, Professor Karim Abdel-Malek for welcoming me to the Virtual Soldier Research (VSR) family and giving me such a great opportunity to contribute to all the fascinating work done here at VSR. I would like to thank Dr. Rajan Bhatt for his invaluable support, encouragement, supervision, patience and useful suggestions throughout my research work. I would also like to thank Dr. Jasbir Arora for his valuable feedback and making learning optimization so interesting and enjoyable. I am especially grateful to Dr. Timothy Marler for his guidance and for believing in me and supporting me throughout my research work. I would like to thank Dr. Salam Rahmatalla for all his help. This project would not have been possible without his work.

I must thank the entire VSR group including Anith Mathai, Hyun Joon Chung, Yujiang Xiang, Anas Nassar, Mohammad Bataineh, Nic Capdevilla and Kim Farrell for all their help and efforts.

Special thanks to the Department of Physics, University of Iowa for helping me when it was needed the most and giving me the opportunity to continue my education. I would also like to thank Jenny Simpson, Deborah Hampton and Courtney Bork for making our graduate life so much easier and helping students focus solely on their studies and work.

Last but not the least, I would like to thank my wife Kranti, my parents and the rest of my family and friends for their love and support and being my strength during this project and throughout my life.

ABSTRACT

Mathematical modeling and realistic human simulation of human jogging motion is a very challenging problem. Majority of the current literature is focused on studying walking or running. This work is aimed at bridging the gap in literature due to the lack of research work in three main areas: (1) simulations and experiments on running at speeds lower than 3 m/s, (2) Kinetics of fore-foot strike pattern in jogging and running and (3) the existence of a double support phase in running at slower speeds and its effects. Formulations to simulate natural human jogging are studied and developed. The digital human model used for this work includes 55 degrees of freedom, 6 for global translation and rotation and 49 for the revolute joints to represent the kinematics of the body. Predictive Dynamics methodology is used for dynamic analysis where the problem is formulated as a nonlinear optimization problem. Both, displacement and forces are considered as unknowns and identified by solving the optimization problem. The equations of motion are satisfied by applying them as equality constraints in the formulation. Kinematics analysis of the mechanical system is performed using the Denavit-Haretneberg (DH) method. The zero moment point (ZMP) condition is satisfied during the ground contact phase to achieve dynamic stability. The joint angle profiles are discretized using B-spline interpolation method. The joint torque squared, also termed dynamic effort, and the difference between predicted motion and motion capture data are used as performance measures and minimized in the optimization formulation. The formulation also includes a set of constraints to simulate natural jogging motion. Two formulations are discussed for jogging on a straight path: (1) one-step jogging formulation and (2) one-stride jogging formulation. The one-stride formulation is discussed for clock-wise and counter clock-wise

jogging along a curved path. Cause and effect is shown by obtaining simulation results for different loading conditions. The proposed formulation provides realistic human jogging motion and is very robust.

PUBLIC ABSTRACT

Mathematical modeling and realistic human simulation of human jogging motion is a very challenging problem. Majority of the current literature is focused on studying walking or running. This work is aimed at bridging the gap in literature due to the lack of research work in three main areas: (1) simulations and experiments on running at speeds lower than 3 m/s, (2) Kinetics of fore-foot strike pattern in jogging and running and (3) the existence of a double support phase in running at slower speeds and its effects. Formulations to simulate natural human jogging are studied and developed. Predictive Dynamics methodology is used for dynamic analysis of the problem. Two formulations are discussed for jogging on a straight path: (1) one-step jogging formulation and (2) one-stride jogging formulation. The one-stride formulation is also discussed for clock-wise and counter clock-wise jogging along a curved path. Cause and effect is studied by obtaining simulation results for different loading conditions. The proposed formulation provides realistic human jogging motion and is very robust.

TABLE OF CONTENTS

LIST OF TABLES	viii
LIST OF FIGURES	ix
CHAPTER 1: INTRODUCTION.....	1
1.1 Motivation	1
1.2 Literature Review	3
1.2.1 Kinematics and Kinetics Studies	3
1.2.2 Simulation Studies.....	5
1.3 Research Objectives and Specific Contributions	6
1.4 Thesis Overview.....	7
CHAPTER 2: PREDICTIVE DYNAMICS	8
2.1 Formulation of Predictive Dynamics	8
2.2 Optimization Design Variables	9
2.3 Objective Function	11
2.4 Constraints.....	12
CHAPTER 3: DYNAMIC PREDICTION OF JOGGING ALONG A STRAIGHT PATH: ONE-STEP FORMULATION	15
3.1 Optimization Formulation	15
3.1.1 Task Description.....	15
3.1.2 Data Collection.....	16
3.1.3 Optimization Design Variables	16
3.1.4 Objective Function for Left Step.....	16
3.1.5 Constraints for Left Step	22
3.1.6 Objective Function for Right Step.....	24
3.1.7 Constraints for Right Step	25
3.2 Results	27
3.2.1 Joint Torque Profiles	28
3.2.2 Ground Reaction Forces	31
3.2.3 Kinematics	34
3.2.4 Cause and Effect Studies	36
CHAPTER 4: DYNAMIC PREDICTION OF JOGGING ALONG A STRAIGHT PATH: ONE-STRIDE FORMULATION	42
4.1 Optimization Formulation	42
4.1.1 Task Description.....	42

4.1.2 Data Collection	42
4.1.3 Optimization Design Variables	43
4.1.4 Objective Function	43
4.1.5 Constraints	44
4.2 Results	48
4.2.1 Joint Torque Profiles	50
4.2.2 Ground Reaction Forces	52
4.2.3 Kinematics	55
4.2.4 Cause and Effect Studies	57
4.2.5 Walking with Increased Velocity	63
CHAPTER 5: DYNAMIC PREDICTION OF JOGGING ALONG A CURVED PATH: ONE-STRIDE FORMULATION	64
5.1 Clock-wise Jogging	64
5.1.1 Optimization Formulation	64
5.1.1.1 Task Description	64
5.1.1.2 Data Collection	65
5.1.1.3 Optimization Design Variables	67
5.1.1.4 Objective Function	67
5.1.1.5 Constraints	68
5.1.2 Results	70
5.1.2.1 Joint Torque Profiles	71
5.1.2.2 Ground Reaction Forces	73
5.1.2.3 Kinematics	76
5.1.2.4 Cause and Effect Studies	78
5.2 Counter Clock-wise Jogging	84
5.2.1 Optimization Formulation	84
5.2.1.1 Task Description	84
5.2.1.2 Data Collection	84
5.2.1.3 Optimization Design Variables	84
5.2.1.4 Objective Function	84
5.2.1.5 Constraints	86
5.2.2 Results	87
5.2.2.1 Joint Torque Profiles	89
5.2.2.2 Ground Reaction Forces	91
5.2.2.3 Kinematics	94
5.2.2.4 Cause and Effect Studies	96
CHAPTER 6: DISCUSSION, CONCLUSIONS AND FUTURE RESEARCH.....	102
6.1 Discussion	102
6.2 Conclusions	104
6.2 Future Work	105
REFERENCES.....	106

LIST OF TABLES

Table 3.1: Symmetry/ Continuity File for Step Formulation.....	19
Table 4.1: Continuity File for Stride Formulation	46

LIST OF FIGURES

Figure 3.1 Continuity condition constraint	27
Figure 3.2 Straight Jogging Left Step Motion Slices at 0, 25, 50, 75 and 100% T	28
Figure 3.3: Comparison of Joint Torque Profiles for Straight Jogging Left Step and Walking Left Step Simulations	30
Figure 3.4: Comparison of Vertical GRF for Straight Jogging Left Step and Walking Left Step Simulations	32
Figure 3.5: Comparison of Fore-Aft GRF for Straight Jogging Left Step and Walking Left Step Simulations.....	33
Figure 3.6: Comparison of Lateral GRF for Straight Jogging Left Step and Walking Left Step Simulations	34
Figure 3.7: Comparison of Joint Angle Profiles for Straight Jogging Left Step and Walking Left Step Simulations.....	35
Figure 3.8: Comparison of Joint Torque Profiles for Straight Jogging Left Step Simulations with No Load, 40 lb Backpack and 80 lb Backpack.....	37
Figure 3.9: Comparison of Vertical GRF for Straight Jogging Left Step Simulations with No Load, 40 lb Backpack and 80 lb Backpack.....	38
Figure 3.10: Comparison of Fore-Aft GRF for Straight Jogging Left Step Simulations with No Load, 40 lb Backpack and 80 lb Backpack.....	39
Figure 3.11: Comparison of Lateral GRF for Straight Jogging Left Step Simulations with No Load, 40 lb Backpack and 80 lb Backpack.....	40
Figure 3.12: Comparison of Joint Angles for Straight Jogging Left Step Simulations with No Load, 40 lb Backpack and 80 lb Backpack.....	41
Figure 4.1 Straight Jogging Stride Motion Slices at 0, 25, 50, 75 and 100% T	49
Figure 4.2: Comparison of Joint Torque Profiles for Straight Jogging Stride and Walking Stride Simulations	51
Figure 4.3: Comparison of Vertical GRF for Straight Jogging Stride and Walking Stride Simulations	53
Figure 4.4: Comparison of Fore-Aft GRF for Straight Jogging Stride and Walking Stride Simulations	54

Figure 4.5: Comparison of Lateral GRF for Straight Jogging Stride and Walking Stride Simulations	55
Figure 4.6: Comparison of Joint Angle Profiles for Straight Jogging Stride and Walking Stride Simulations.....	56
Figure 4.7 Comparison of Joint Torque Profiles for Straight Jogging Stride Simulations with No Load, 40 lb Backpack and 80 lb Backpack.....	58
Figure 4.8 Comparison of Vertical GRF for Straight Jogging Stride Simulations with No Load, 40 lb Backpack and 80 lb Backpack.....	59
Figure 4.9 Comparison of Fore-Aft GRF for Straight Jogging Stride Simulations with No Load, 40 lb Backpack and 80 lb Backpack.....	60
Figure 4.10 Comparison of Lateral GRF for Straight Jogging Stride Simulations with No Load, 40 lb Backpack and 80 lb Backpack.....	61
Figure 4.11 Comparison of Joint Angles for Straight Jogging Stride Simulations with No Load, 40 lb Backpack and 80 lb Backpack.....	62
Figure 4.12 Walking Stride Simulation with Velocity 2 m/s and Step Length 0.5 m Motion Slices at 0, 25, 50, 75 and 100% T.....	63
Figure 5.1 Points on the foot for foot contact position constraint	65
Figure 5.2 Foot location along the curve	66
Figure 5.3 CW Jogging Stride Motion Slices at 0, 25, 50, 75 and 100% T.....	71
Figure 5.4: Comparison of Joint Torque Profiles for Straight Jogging Stride and Clock-wise Jogging Stride Simulations.....	72
Figure 5.5: Comparison of Vertical GRF for Straight Jogging Stride and Clock-wise Jogging Stride Simulations	74
Figure 5.6: Comparison of Fire-Aft GRF for Straight Jogging Stride and Clock-wise Jogging Stride Simulations	75
Figure 5.7: Comparison of Lateral GRF for Straight Jogging Stride and Clock-wise Jogging Stride Simulations	76
Figure 5.8: Comparison of Joint Torque Profiles for Straight Jogging Stride and Clock-wise Jogging Stride Simulations.....	77
Figure 5.9: Comparison of Joint Torque Profiles for Clock-wise Jogging Stride Simulations with No Load, 40 lb Backpack and 80 lb Backpack.....	79

Figure 5.10: Comparison of Vertical GRF for Clock-wise Jogging Stride Simulations with No Load, 40 lb Backpack and 80 lb Backpack.....	80
Figure 5.11: Comparison of Fore-Aft GRF for Clock-wise Jogging Stride Simulations with No Load, 40 lb Backpack and 80 lb Backpack.....	81
Figure 5.12: Comparison of Lateral GRF for Clock-wise Jogging Stride Simulations with No Load, 40 lb Backpack and 80 lb Backpack.....	82
Figure 5.13: Comparison of Joint Angles for Clock-wise Jogging Stride Simulations with No Load, 40 lb Backpack and 80 lb Backpack.....	83
Figure 5.14: CCW Jogging Stride Motion Slices at 0, 25, 50, 75 and 100% T.....	88
Figure 5.15: Comparison of Joint Torque Profiles for Straight Jogging Stride and Counter Clock-wise Jogging Stride Simulations	90
Figure 5.16: Comparison of Vertical GRF for Straight Jogging Stride and Counter Clock-wise Jogging Stride Simulations.....	92
Figure 5.17: Comparison of Fore-Aft GRF for Straight Jogging Stride and Counter Clock-wise Jogging Stride Simulations	93
Figure 5.18: Comparison of Lateral GRF for Straight Jogging Stride and Counter Clock-wise Jogging Stride Simulations.....	94
Figure 5.19: Comparison of Joint Angles for Straight Jogging Stride and Counter Clock-wise Jogging Stride Simulations.....	95
Figure 5.20: Comparison of Joint Torque Profiles for Counter Clock-wise Jogging Stride Simulations with No Load, 40 lb Backpack and 80 lb Backpack.....	97
Figure 5.21: Comparison of Vertical GRF for Counter Clock-wise Jogging Stride Simulations with No Load, 40 lb Backpack and 80 lb Backpack.....	98
Figure 5.22: Comparison of Fore-Aft GRF for Counter Clock-wise Jogging Stride Simulations with No Load, 40 lb Backpack and 80 lb Backpack.....	99
Figure 5.23: Comparison of Lateral GRF for Counter Clock-wise Jogging Stride Simulations with No Load, 40 lb Backpack and 80 lb Backpack.....	100
Figure 5.24: Comparison of Joint Angles for Counter Clock-wise Jogging Stride Simulations with No Load, 40 lb Backpack and 80 lb Backpack.....	101

CHAPTER 1: INTRODUCTION

1.1 Motivation

The field of digital human modeling and simulation has seen a tremendous increase in its popularity and applications in the recent years. It has become an integral part of a product development cycle for many industries. It has made the design process much faster, easier and less costly. In this field of virtual humans, it is very important to study and predict human performance. Human motion prediction refers to the simulation of interaction of different user populations with a variety of environments. This prediction is achieved by an optimization-based method in which the body's degrees of freedom (DOF) are treated as the design variables to achieve the required motion and some performance measure is used as the objective function. The predicted motion must complete tasks while resembling the reference motion and maintaining dynamic equilibrium of the digital human. All these constraints along with the non-linear nature of the equations of motion make dynamic motion prediction (DMP) a very challenging problem.

Extensive work has been done toward developing powerful motion prediction schemes that could perform in a task-based manner. Forward dynamics (FD) is a method that calculates the motion of the body based on known forces or torques. Inverse dynamics (ID) is a method for computing forces and/or moments of force (torques) based on the kinematics (motion) of a body and the body's inertial properties. ID and FD provide a mathematical representation of the dynamic and kinematic properties of the human model. The motion simulation process is formulated as a constrained optimization problem (Kim, J. 2006) with the physical constraints depicting the task descriptions. But these methods involve the integration of equations of motion (Roussel, L. 1998) (Chevallereau, C., and

Aoustin, Y. 2001). Moreover, for many dynamic systems and especially human motion, both forces and motion are unavailable. Hence, the work presented here uses the predictive dynamics (PD) methodology presented by Xiang (2008) that uses a recursive formulation with forces and motion parameters as unknowns and equations of motion as equality constraints. The method is applied to a 55 DOF model. It is an optimization-based approach with physics-based constraints.

The primary goal of this work is to study the human jogging motion using digital human models. An additional hypothesis that is tested in this work is that simulation of human jogging by formulating the motion as a separate problem with different gait cycle phases and foot striking patterns as compared to walking provides more realistic motion. Extensive research has been done on studying human walking or running at speeds higher than 3 m/s but there has not been much work done on studying running at speeds less than 3 m/s. Literature on simulating natural human jogging motion and its analysis is even less so. A full body dynamic simulation of human jogging is not available in the literature.

Majority of the literature uses the same gait profile for jogging as running with no double support phase. However, Kalron et.al (2013) showed that, although minimal (up to 0.5 % gait cycle), healthy subjects did show a double support phase while jogging. The study compared gait and jogging parameters in healthy subjects and people with minimally impaired multiple sclerosis (MS). Gazendam and Hof (2007) studied electromyography (EMG) profiles in jogging and running at different speeds and reported an increased stance phase (46-57%) in jogging as compared to normal running (30-37%). The study showed the practicality of defining an additional mode of human locomotion termed jogging that does not include a swing or aerial phase. Novacheck (2008) reported that about 80% of

distance runners are rear-foot strikers and hence majority of the research has focused on running formulations with rear-foot strike patterns. Lieberman et.al (2010) studied foot strike patterns and collision forces in barefoot versus shod runners and showed that fore-foot strike generates smaller collision forces and may protect the feet and lower limbs from some of the impact-related injuries now experienced by a high percentage of runners. There still exists a lack of literature on the analysis of running with fore-foot strike pattern. Thus, this research work proposes jogging with double support phase and fore-foot strike to address this critical need.

1.2 Literature Review

Jogging is defined as a form of running at slower speeds of 4 – 6 mph or 1.8 – 2.7 m/s. Very few researchers have worked on the mathematical modeling of digital human jogging simulation. Thus, there exists a real lack of relevant literature that is directly related to the digital human jogging simulation problem. Extensive research work has been done in studying the kinematics and kinetics of walking and running motions which can be reviewed to obtain some insights into the jogging problem. Robotic simulations of walking and running motion have also been performed.

1.2.1 Kinematics and Kinetics Studies

Kinematics and kinetics studies of human locomotion provide important results and play a huge role in the validation of digital human motion simulation. Many experiments have been performed in the biomechanics area to measure the joint angle profiles, the joint torque profiles and the ground reaction forces (GRF). Biomechanics of human running has

been reviewed in many papers (Ounpuu, 1994, Novacheck, 1998). Ounpuu (1994) defined the general gait terminology such as gait cycle, step length and stride length along with description of the kinematics, kinetics and ground reaction forces of human walking and running. Novacheck (1998) described gait cycle, kinematics, kinetics, EMG and potential and kinetic energy of running. Demura et.al (2010) compared gait properties during level walking with varying loads on the back and showed that double support times increase significantly with increasing load. Harman et.al (2000) studied the effects of interaction between different backpack loads and walking speeds on the biomechanics of load carriage tasks. In the analysis of support phases in human locomotion, GRFs are frequently used as a primary descriptive component. Finch et.al (1995) studied differences in ground reaction forces when walking in a circle as compared to straight walking. Consistent loading patterns observed in the study indicated that walking about a 3.66 m diameter circle was same as straight walking. Cavanagh, Williams and Clarke (1981) reported magnitudes of 1.1 to 1.3 times the body weight (BW) for vertical GRF loading in walking task. Sasaki et.al (2006) looked at differences in muscle function during walking and running at same speeds.

Cross (1998) studied the vertical ground reaction forces of standing, walking, running and jumping on a force plate including jogging at 3 m/s. However, no data was provided for jogging below 3 m/s. Kuntz and Terauds (1983) performed force measurements for jogging using biomechanics cinematography but the actual speed of jogging was not reported. Keller studied the relationship between vertical ground reaction forces and speed during walking, slow jogging and running. It was shown that the vertical ground reaction forces increased linearly during walking and running from 1.2 BW to

approximately 2.5 BW at 6m/s. The results suggested that slow or fast running with a lower, fixed center of gravity decreases impact forces. Nigg et.al (1987) found similar results for 3-6 m/s but did not consider running at speeds less than 3 m/s. Gait speed was also studied in many investigations (Nigg et.al (1987), Cavanagh (1980), Munro et.al. (1987), and Frederick (1980)) but was generally limited to a small range of walking or running velocities. Ounpuu (1994) reported GRFs ranging from 1.3 – 1.5 BW in walking to 2 – 3 BW in running. Novacheck (1998) also reported GRFs of 3 times BW and higher for running. Hamill et.al (1983) studied the variations in ground reaction force parameters at different running speeds and observed a change in the magnitude of forces as a result of changes in running speed. However, running velocities less than 4 m/s were not considered in the study. Hart et.al (2009a) analyzed effects of fatigue on jogging kinematics in healthy as well as low back pain suffering participants. Castro et.al (2013) studied the relationship between running intensity, muscle activation and stride kinematics as running speeds were increased from 10 km/h to 16km/h or 2.8 m/s to 4.4 m/s. Smoliga et.al (2014) reported physiological parameters during running at 2.4 m/s on a non-motorized curved treadmill. Dwyer et.al (2012) proposed standard definitions (velocity ranges) for walking, jogging and running for field sports athletes using time motion analysis. Burgess et.al (2006) and Dogramaci and Watsford (2006) presented velocity ranges for different locomotor categories with median velocity of 2 m/s for jogging.

1.2.2 Simulation Studies

Hodgins (1996) simulated 3D virtual human running for speeds of 2.5 to 5 m/s. However, the study was for animation purposes where stability and joint torque limits of a

human were not considered. Sasaki and Neptune (2006) performed forward dynamical simulations of walking and running at the preferred transition speed (PTS, Raynor et.al, 2002) of 2 m/s for a 2D bipedal musculoskeletal model to study the differences in muscle function. Celik and Piazza presented a simulation of aperiodic sprinting using a modified spring-loaded inverted pendulum (SLIP) biped model. Sequential quadratic programming method was used to solve the non-linear programming problem. Chung (2009) presented optimization-based dynamic simulation of 3D human running using PD and also studied slow human jogging motion on a curvilinear path.

Lens et.al simulated the dynamics of a legged robot to demonstrate ground contact forces during slow jogging motion. However, only the lower body was considered with very few degrees of freedom. Grizzle (2009) introduced a new robotic bipedal walker and runner named Mabel but it considered very few DOF (9 DOF model). Locomotion simulations were also performed on Honda ASIMO (Hirai et al., 1998) and Sony QRIO (Nagasaka et al., 2004) robots but again the number of DOF considered were very few and the anthropometric data used by the mathematical models did not resemble that of a human.

1.3 Research Objectives and Specific Contributions

The primary objective of this study is the formulation and prediction of realistic human jogging motion on a straight and curved path, analysis of the underlying dynamics and to observe the effects of external loading on the motion. Specific contributions of this research work are summarized as follows:

1) Human jogging motion on a straight path is simulated using the one-step formulation.

2) Human jogging motion on a straight path is simulated using the one-stride formulation.

3) Clock-wise and counter clock-wise jogging motion along a curved path is simulated using the one-stride formulation.

4) Different loading conditions are and its effects were studied on the jogging motion using predictive dynamics.

5) It was shown that simulation of human jogging by formulating the motion as a separate problem with different gait cycle phases and foot striking patterns as compared to walking provides more realistic motion.

1.4 Thesis Overview

In Chapter 2, the concept of predictive dynamics is presented. The basic notion and formulation of predictive dynamics is defined along with the constraints and objective functions used. In Chapter 3, the one-step formulation of human jogging motion on a straight path is presented. The results for various simulations along with cause and effect studies are provided. In Chapter 4, the one-stride formulation of human jogging motion on a straight path is presented. The results for various simulations are also presented. In Chapter 5, the one-stride formulation of human jogging motion on a curved path is presented. The results for simulations of clock-wise and counter clock-wise jogging along with cause and effect studies are provided. In Chapter 6, conclusions and future work are discussed.

CHAPTER 2: PREDICTIVE DYNAMICS

Predictive Dynamics (Xiang et.al, 2010a) refers to human motion prediction in a physics-based world. In general, forward and inverse dynamics have been used to solve mechanical problems where either information about force or information about displacement, velocity and acceleration is available. However, a bio-system such as human motion has very limited information which means that information about force and information about displacement, velocity, and acceleration is unavailable. For instance, only state responses and a few boundary conditions are available and joint angle profiles and joint torque profiles are unknown. Predictive dynamics can be applied to solve the problem in such a scenario.

The digital human, SANTOS, used for this work, has been developed at the Virtual Soldier Research (VSR) lab at the University of Iowa. It is modeled as a mechanical system that includes link lengths, mass moments of inertia, joint torques and external forces. The entire model includes 55 degrees of freedom, 6 for global translation and rotation and 49 for the revolute joints to represent the kinematics of the body. The Denavit-Hartenberg (DH) method (Denavit and Hartenberg, 1955) is applied for the kinematics analysis.

2.1 Formulation of Predictive Dynamics

An optimization-based approach in a physics environment forms the basis of predictive dynamics. It is capable of handling complicated dynamics problems with a large number of degrees of freedom. However, a performance measure needs to be formulated for the optimization-based approach which is generally unknown for a bio-system. A few

performance measures have been studied in the literature for general human motion, such as the dynamics effort based on energy consumption. It is also very helpful to test the feasibility of constraints and obtaining a good starting point for the optimization process. Motion capture data is used to provide an initial feasible kinematics solution and then dynamics performance measure is added to the objective function to solve the problem. Constraints formulation for the optimization problem is another difficult process since there is little information available for the human motion to be simulated. Some constraints may be obtained from the motion capture data and any literature available on the task while some constraints may be imposed based on assumptions. There are two types of constraints: (1) time-dependent constraints that must be satisfied over the entire time domain and (2) time-independent constraints which need to be satisfied only at a specific time.

2.2 Optimization Design Variables

For the optimization problem, cubic B-spline function is used to discretize the time domain. Thus a parameterized joint angle profile $q(t)$ can be defined as follows:

$$q_i(t, \mathbf{t}, \mathbf{P}) = \sum_{j=0}^m N_j(t, \mathbf{t}) p_{ij} \quad 0 \leq t \leq T \quad (2.1)$$

where t is the time instant, $N_j(t, \mathbf{t})$ are the basis functions, $\mathbf{t} = \{t_0, \dots, t_s\}$ is the knot vector ($s+1$ discretized time points), and $\mathbf{P}_{ij} = \{p_{i0}, \dots, p_{im}\}$ is the control points vector for the i^{th} joint angle profile and $m+1$ is the number of control points. The B-spline consistency condition (De Boor, 2001) needs to be satisfied by s and m . Thus, the value of the control points can be changed to modify the shape of the joint angle profiles. The control points

are treated as the optimization or design variables in this representation. The knot vector is specified and fixed for the optimization process in this work. Six control points are used for the step formulation and nine control points are used for the stride formulation for each DOF. Thus there are a total of 330 design variable (55x6) for the step formulation and 495 design variables (55x9) for the stride formulation. The final solution and its computation time are directly affected by the number of control points used in the formulation. Joint angle trajectories a motion require smoothness and flexibility. B-spline functions provide many important properties such as differentiability, continuity and local control. These properties make B-splines appropriate for representing joint angle profiles.

The jogging task is formulated as a general nonlinear programming (NLP) problem: to find the optimal control points vector \mathbf{P} for the jogging motion to minimize a human performance measure, $f(\mathbf{P})$, subject to physical constraints as follows:

$$\begin{aligned}
 &\text{Find : } \mathbf{P} \\
 &\text{To : } \min f(\mathbf{P}) \\
 &\text{Sub. } h_i = 0, \quad i = 1, \dots, p \\
 &\quad \quad g_j \leq 0, \quad j = 1, \dots, m
 \end{aligned} \tag{2.2}$$

where h_i are the equality constraints such as the equations of motion and g_j are the inequality constraints such as joint and torque limits. Expressions for f , h_i and g_j are given in the following paragraphs.

2.3 Objective Function

Motion capture data has been used in this work to improve motion simulation. The difference or error between the desired joint angles from motion capture and the actual joint angles forms the first performance criterion. It is also termed as the tracking error and is minimized in the optimization formulation.

$$f_1 = \sum_{i=1}^{ndof} \int_{t=0}^T (q_{id}(t) - q_i(t))^2 dt \quad (2.3)$$

where $ndof$ is the number of DOF, q_{id} is the desired joint angle vector for the i_{th} DOF and q_i is the actual joint angle vector for the i_{th} DOF.

The time integral of the squares of all joint torques, also termed as dynamic effort, is used as the other performance criterion for the jogging motion (Fregly 2007, Xiang et al. 2010a):

$$f_2 = \sum_{i=1}^{ndof} \int_{t=0}^T \left(\frac{\tau_i}{|\tau|_{max}} \right)^2 dt \quad (2.4)$$

where $|\tau|_{max}$ is the maximum absolute value of all the joint torque limits; $ndof$ is the number of DOF; T is the last time point, i.e., total time.

The overall objective function is a weighted combination of the two performance measures stated above.

$$f(\mathbf{P}) = (w_1 * f_1) + (w_2 * f_2) \quad (2.5)$$

where w_1 and w_2 are the weights for the objective functions. Tracking error is minimized to get an initial kinematics solution with $w_1=1$ and $w_2=0$ which is used as the starting point

when dynamic effort is added with $w_1 = 0.5$ and $w_2 = 0.5$. The weights for the objective functions are selected such that $\sum w_i = 1$.

2.4 Constraints

The behavior of a physical system can be described using the equations of motion. The general equations of motion for the Santos model are written as

$$f(q, \dot{q}, \ddot{q}, t) = \tau \quad (2.6)$$

where $q, \dot{q}, \ddot{q} \in R^N$ are the state variables i.e. joint displacements, velocities and accelerations and $\tau \in R^N$ are the generalized forces and N is the number of DOF for the model. Equations of motion are imposed as equality constraints in the predictive dynamics optimization formulation.

Two types of constraints are considered for the jogging optimization problem as specified before: time-dependent and time-independent constraints. The time-dependent constraints include (1) joint angle limits; (2) joint torque limits; (3) Ground penetration and (4) ZMP stability. These constraints are detailed as follows:

(1) Joint angle limits

The physical range of motion of joints accounts for the joint angle limits (Xiang et al. 2010a).

$$\mathbf{q}^L \leq \mathbf{q}(t) \leq \mathbf{q}^U, \quad 0 \leq t \leq T \quad (2.7)$$

(2) Joint torque limits

The dynamic physical strength of joints accounts for the joint torque limits where the maximum strength (τ_i^L (*lower*) or τ_i^U (*upper*)) of a particular joint, i , of a person changes with a change in its joint angle position $q(t)$ and velocity $\dot{q}(t)$.

$$\tau_i(q(t), \dot{q}(t))^L \leq \tau_i(t) \leq \tau_i(q(t), \dot{q}(t))^U; 0 \leq t \leq T; i = 1, \dots, ndof \quad (2.8)$$

Given the complexity associated with the calculation of dynamic strength, it is only applied to a set of prominent joints namely the spine, knee, elbow and hip. Static joint limits are applied to the remaining DOF. The data for the static strength is obtained from literature (Xiang et al. 2012a) and the constraint is simplified as follows:

$$\tau_i^L \leq \tau_i(t) \leq \tau_i^U \quad ; \quad 0 \leq t \leq T; \quad i = 1, \dots, ndof \quad (2.9)$$

The constraint is further normalized so that the minimum value of the normalized function is -1 and the maximum value of the normalized function is +1 to help with the gradient based optimization process. Hence, the static torque limit constraint is implemented in the code as follows:

$$-1 \leq \frac{\tau_i(t) - \tau_i^L}{\tau_i^U - \tau_i^L} \leq 1 \quad ; \quad 0 \leq t \leq T; \quad i = 1, \dots, ndof \quad (2.10)$$

(3) Ground penetration

The absolute height ($y_i(t)$) and speed ($v_i(t)$) of contacting points are zero when the foot is in contact with the ground. The contacting points should be above the ground and their height is greater than zero at all other times. This constraint is formulated as follows:

$$\begin{aligned} y_i(t) &= 0, \quad v_i(t) = 0, \quad 0 \leq t \leq T, \quad i \in \text{contact} \\ y_j(t) &\geq 0, \quad 0 \leq t \leq T, \quad j \notin \text{contact} \end{aligned} \quad (2.11)$$

where contact contains a list of foot contacting points.

(4) ZMP stability

The stability condition is imposed by locating ZMP position in the foot supporting region (FSR) as follows (Xiang et al. 2010a):

$$z_{ZMP}(t) \in FSR, \quad y_{ZMP}(t) \in FSR, \quad 0 \leq t \leq T \quad (2.12)$$

Time independent constraints are as follows:

(1) Foot contacting positions

Foot contacting positions during the motion are specified based on the step length L to satisfy the step length constraint. The optimization process determines the initial and final postures, velocities and accelerations.

(2) Continuity/ Symmetry conditions

$$\begin{aligned} q_i(0) - q_i(T) &= 0, & i &= 2, 3, \dots, n \\ \dot{q}_j(0) - \dot{q}_j(T) &= 0, & j &= 1, 2, \dots, n \\ |\ddot{q}_k(0) - \ddot{q}_k(T)| &\leq \varepsilon, & k &= 1, 2, \dots, n \end{aligned} \quad (2.13)$$

where n is the number of DOFs and ε is a positive number ranging from 0.001 to 10. The position continuity constraint is excluded for the first DOF which corresponds to global translation along the jogging direction. In some cases, a smaller value for ε for the acceleration continuity constraint may result in an infeasible solution indicating a conflict with other constraints. Hence, a large value for ε may be used for the constraint to account for the discontinuities resulting due to the impulse-like forces at toe-strike. Continuity constraint is applied to the stride formulation where initial and final postures of the motion are same. Symmetry constraint is used for the step formulation where the final posture mirrors the initial posture.

CHAPTER 3: DYNAMIC PREDICTION OF JOGGING ALONG A STRAIGHT PATH: ONE-STEP FORMULATION

In this chapter, normal jogging simulation along a straight path is presented using the one-step formulation. The left step problem is solved first and its initial and final postures are used as input for the symmetry constraint to solve the right step problem. The problem is formulated as a nonlinear optimization problem. The laws of physics are enforced by evaluating the equations of motion in the optimization process using inverse dynamics. SNOPT, a commercial software based on sequential quadratic programming (SQP) is used to solve the problem (Gill, Murray, and Saunders, 2002). Besides normal jogging, the effects of external loading are also observed. The joint torques and ground reaction forces are obtained from the simulations and studied.

3.1 Optimization Formulation

3.1.1 Task Description

The task is described as follows: Given a marker, Santos jogs towards the marker on a straight path. Although, it is an asymmetric task with Santos jogging with a gun in his left hand, the one-step formulation is tested since it provides flexibility in terms of the task simulation. Since the distance to be covered is unknown, the number of steps required to reach the desired position are unknown. The step formulation allows simulation of odd number of steps for this task. In this formulation, the left step is solved first and then its initial and final postures are used as input for the right step to solve the problem.

3.1.2 Data Collection

A velocity of 2 m/s is used for the task. The anthropometry (height and weight) of the subject is used as an input. Based on the velocity and the subject height, the step length L is calculated according to the following equation (Bruderlin and Calvert, 1996):

$$L = 0.1394 + (0.00465 + level) * v * \sqrt{\frac{body_height}{1.8}} \text{ m} \quad (3.1)$$

where v is running speed in m/min, $level$ is the level of expertise in running ranging from -0.001 for poor to 0.001 for skilled based on the observation that better runners have a greater stride length at a given velocity than less skilled or poor runners; and $body_height$ is the height of the human body (in meters). The time duration for the step is then calculated as $T=L/v$.

3.1.3 Optimization Design Variables

The joint angle profiles $\mathbf{q}(t)$ parameterized using B-spline approximation are used as design variables for the optimization problem.

3.1.4 Objective Function for Left Step

Motion capture data has been used in this work to improve motion simulation. The squared difference or error between the desired joint angles from motion capture and the actual joint angles forms the first performance criterion. It is also termed as the tracking error and is minimized in the optimization formulation. It is defined as follows:

$$f_1 = \sum_{i=1}^{ndof} \int_{t=0}^T (q_{id}(t) - q_i(t))^2 dt \quad (3.2)$$

where $ndof$ is the number of DOF, q_{id} is the desired joint angle vector for the i th DOF and q_i is the actual joint angle vector for the i th DOF. Since joint angles are in radians and the tracking objective has a very small value, the tracking objective function is not normalized. The joint angle values are maintained within $\pm\pi$ to avoid unwarranted rotations in motion due to the motion capture data which may have values higher than π .

Using motion capture data provides a more realistic simulation of the motion. It also helps to reduce the number of constraints applied to the optimization problem. For instance, constraints such as arm-leg coupling for a symmetric motion, self-avoidance and even ground penetration on the velocity level are not required in the presence of motion capture data. On the other hand, obtaining motion capture data is very time consuming and expensive. It can take weeks to capture the data and process it before it can be used for motion simulation. Also the motion capture data only represents a particular subject with a specific anthropometry. Hence, it is not sufficient to just use motion capture as the performance criterion in the optimization problem to simulate the effects of external loads and different anthropometries.

The time integral of the squares of all joint torques, also termed as dynamic effort, is used as the other performance criterion for the jogging motion (Fregly 2007, Xiang et al. 2010a):

$$f_2 = \sum_{i=1}^{ndof} \int_{t=0}^T \left(\frac{\tau_i}{|\tau|_{max}} \right)^2 dt \quad (3.3)$$

where $|\tau|_{\max}$ is the maximum absolute value of all the joint torque limits; $ndof$ is the number of DOF; T is the last time point, i.e., total time. The torque objective is normalized since it can take very high values especially compared to the tracking objective values. Xiang (2008) showed that the energy related performance measure of the dynamic effort is most appropriate to predict dynamic human motion since natural motion always obeys an energy-saving rule. The effect of external loading and varying anthropometries is simulated successfully using the dynamic effort objective function. This is in accordance with the notion that people always choose a strategy to perform any task that is more efficient in increasing stability and reducing the effort associated with the task especially when subjected to external loads. This will also be seen in the successful simulation of jogging for a male avatar whose anthropometric properties are different from that of the male subject used for motion capture data.

A third objective function called the position-symmetry objective is introduced for the left step. Since the jogging motion to be simulated is asymmetric, position symmetry cannot be applied as a hard constraint. However, symmetry needs to be applied to the problem at the position level in some way to obtain a smooth motion especially for cases with external loads. Whether symmetry or continuity is applied is decided based Table 3.1 where 0 refers to no symmetry, 1 refers to continuity and -1 refers to symmetry. Hence position symmetry is introduced as an objective function. It is defined as follows:

$$f_3 = \sum (q_L(0) - q_R(T))^2 \quad (3.4)$$

where subscripts L and R refer to the left and right side of the body. It includes DOF for which symmetry is applied according to Table 3.1. Arms and shoulder are excluded from the objective to maintain the asymmetry in the arm motion.

Table 3.1: Symmetry/ Continuity File for Step Formulation

DOF	Symmetry/ Continuity Condition
GT1	0
GT2	-1
GT3	1
GR1	-1
GR2	1
GR3	-1
SpineLow_LeftRightBend	-1
SpineLow_ExtensionFlexion	1
SpineLow_RightLeftRotation	-1
SpineMidLow_LeftRightBend	-1
SpineMidLow_ExtensionFlexion	1
SpineMidLow_RightLeftRotation	-1
SpineMidHigh_LeftRightBend	-1
SpineMidHigh_ExtensionFlexion	1
SpineMidHigh_RightLeftRotation	-1
SpineHigh_LeftRightBend	-1

SpineHigh_ExtensionFlexion	1
SpineHigh_RightLeftRotation	-1
RightClavicle_ElevationDepressionShrug	-1
RightClavicle_RetractionProtraction	-1
RightShoulder_AbductionAdduction	-1
RightShoulder_ExtensionForwardFlexion	-1
RightShoulder_InternalRotationExternalRotation	-1
RightElbow_FlexionExtension	-1
RightWrist_PronationSupination	-1
RightWrist_RadialUlnarDeviation	-1
RightWrist_ExtensionFlexion	-1
LeftClavicle_ElevationDepressionShrug	1
LeftClavicle_RetractionProtraction	1
LeftShoulder_AbductionAdduction	1
LeftShoulder_ExtensionForwardFlexion	1
LeftShoulder_InternalRotationExternalRotation	1
LeftElbow_FlexionExtension	1
LeftWrist_PronationSupination	1
LeftWrist_RadialUlnarDeviation	1
LeftWrist_ExtensionFlexion	1
LowerNeck_LeftRightBending	-1
LowerNeck_ExtensionFlexion	1
LowerNeck_RightLeftRotation	-1

UpperNeck_LeftRightBending	-1
UpperNeck_ExtensionFlexion	1
RightHip_AbductionAdduction	-1
RightHip_FlexionExtension	-1
RightHip_ExternalRotationInternalRotation	-1
RightKnee_ExtensionFlexion	-1
RightAnkle_DorsiPlantarFlexion	-1
RightAnkle_EversionInversion	-1
RightMidFootLateral_ExtensionFlexion	-1
LeftHip_AbductionAdduction	-1
LeftHip_FlexionExtension	-1
LeftHip_ExternalRotationInternalRotation	-1
LeftKnee_ExtensionFlexion	-1
LeftAnkle_DorsiPlantarFlexion	-1
LeftAnkle_EversionInversion	-1
LeftMidFootLateral_ExtensionFlexion	-1

The overall objective function is a weighted combination of the three performance measures stated above.

$$f(\mathbf{P}) = (w_1 * f_1) + (w_2 * f_2) + (w_3 * f_3) \quad (3.5)$$

where w_1 , w_2 and w_3 are the weights for the objective functions. For the reasons mentioned above, the motion capture objective cannot be used on its own to simulate human motion.

On the other hand, it does provide a more realistic motion and although there are differences in the anthropometry, a majority of the joint angles are very similar for a given task especially for the no load case. The dynamic effort on its own would require additional constraints to simulate the motion and would provide less realistic results. Hence, equal weightage is given to the two primary objectives. Tracking error is minimized to get an initial kinematics solution with $w_1 = 1$, $w_2 = 0$ and $w_3 = 0$ which is used as the starting point when the other two objective functions are added with $w_1 = 0.4$, $w_2 = 0.4$ and $w_3 = 0.2$. The weights for the objective functions are selected such that $\sum w_i = 1$.

3.1.5 Constraints for Left Step

Two types of constraints are considered for the jogging optimization problem as specified before: time-dependent and time-independent constraints. The time-dependent constraints include (1) joint angle limits; (2) joint torque limits; and (3) Zero moment point (ZMP) stability. These constraints are detailed as follows:

(1) Joint angle limits

The physical range of motion of joints accounts for the joint angle limits (Xiang et al. 2010a).

$$\mathbf{q}^L \leq \mathbf{q}(t) \leq \mathbf{q}^U, \quad 0 \leq t \leq T \quad (3.6)$$

(2) Joint torque limits

The dynamic physical strength of joints accounts for the joint torque limits where the maximum strength (τ_i^L or τ_i^U) of a particular joint, i , of a person changes with a change in its joint angle position $q(t)$ and velocity $\dot{q}(t)$.

$$\tau_i(q(t), \dot{q}(t))^L \leq \tau_i(t) \leq \tau_i(q(t), \dot{q}(t))^U; 0 \leq t \leq T; i = 1, \dots, ndof \quad (3.7)$$

(3) ZMP stability

The stability condition is imposed by locating ZMP position in the foot supporting region (FSR) as follows (Xiang et al. 2010a):

$$z_{ZMP}(t) \in FSR, y_{ZMP}(t) \in FSR, \quad 0 \leq t \leq T \quad (3.8)$$

Time independent constraints are as follows:

(1) Foot contacting positions

Foot contacting positions during the motion are specified based on the step length L to satisfy the step length constraint. The optimization process determines the initial and final postures, velocities and accelerations.

(2) Symmetry constraint

Symmetry at the velocity and acceleration level is applied as a constraint. Again, the arms and shoulders are excluded to maintain asymmetry in the arm motion.

$$q'_L(0) - q'_R(T) = 0; q''_L(0) - q''_R(T) = 0 \quad (3.9)$$

where subscripts L and R refer to the left and right side of the body. It includes DOF for which symmetry is applied according to Table 3.1. Arms and shoulder are excluded from the objective to maintain the asymmetry in the arm motion.

3.1.6 Objective Function for Right Step

Motion capture data has been used in this work to improve motion simulation. The squared difference or error between the desired joint angles from motion capture and the actual joint angles forms the first performance criterion. It is also termed as the tracking error and is minimized in the optimization formulation.

$$f_1 = \sum_{i=1}^{ndof} \int_{t=0}^T (q_{id}(t) - q_i(t))^2 dt \quad (3.10)$$

where $ndof$ is the number of DOF, q_{id} is the desired joint angle vector for the i th DOF and q_i is the actual joint angle vector for the i th DOF.

The time integral of the squares of all joint torques, also termed as dynamic effort, is used as the other performance criterion for the jogging motion (Fregly 2007, Xiang et al. 2010a):

$$f_2 = \sum_{i=1}^{ndof} \int_{t=0}^T \left(\frac{\tau_i}{|\tau|_{max}} \right)^2 dt \quad (3.11)$$

where $|\tau|_{max}$ is the maximum absolute value of all the joint torque limits; $ndof$ is the number of DOF; T is the last time point, i.e., total time.

The overall objective function is a weighted combination of the two performance measures stated above.

$$f(\mathbf{P}) = (w_1 * f_1) + (w_2 * f_2) \quad (3.12)$$

where w_1 and w_2 are the weights for the objective functions. Tracking error is minimized to get an initial kinematics solution with $w_1 = 1$ and $w_2 = 0$ which is used as the starting point when dynamic effort is added with $w_1 = 0.5$ and $w_2 = 0.5$. The weights for the objective functions are selected such that $\sum w_i = 1$.

3.1.7 Constraints for Right Step

Two types of constraints are considered for the jogging optimization problem as specified before: time-dependent and time-independent constraints. The time-dependent constraints include (1) joint angle limits; (2) joint torque limits; and (3) ZMP stability. These constraints are detailed as follows:

(1) Joint angle limits

The physical range of motion of joints accounts for the joint angle limits (Xiang et al. 2010a).

$$\mathbf{q}^L \leq \mathbf{q}(t) \leq \mathbf{q}^U, \quad 0 \leq t \leq T \quad (3.13)$$

(2) Joint torque limits

The dynamic physical strength of joints accounts for the joint torque limits where the maximum strength (τ_i^L or τ_i^U) of a particular joint, i , of a person changes with a change in its joint angle position $q(t)$ and velocity $\dot{q}(t)$.

$$\tau_i(q(t), \dot{q}(t))^L \leq \tau_i(t) \leq \tau_i(q(t), \dot{q}(t))^U; \quad 0 \leq t \leq T; \quad i = 1, \dots, ndof \quad (3.14)$$

(3) ZMP stability

The stability condition is imposed by locating ZMP position in the foot supporting region (FSR) as follows (Xiang et al. 2010a):

$$z_{ZMP}(t) \in FSR, \quad y_{ZMP}(t) \in FSR, \quad 0 \leq t \leq T \quad (3.15)$$

Time independent constraints are as follows:

(1) Foot contacting positions

Foot contacting positions during the motion are specified based on the step length L to satisfy the step length constraint. The optimization process determines the initial and final postures, velocities and accelerations.

(2) Continuity/ Symmetry condition

The left and the right step are put together using the continuity constraint Chung (2009). Initial and final postures of the first optimization (left step) are matched with final and initial posture of the second optimization (right step) respectively. The constraint is depicted in figure 5.3 and is mathematically described as:

$$\mathbf{q}_{left}(0) = \mathbf{q}_{right}(T); \quad \mathbf{q}_{left}(T) = \mathbf{q}_{right}(0) \quad (3.16)$$

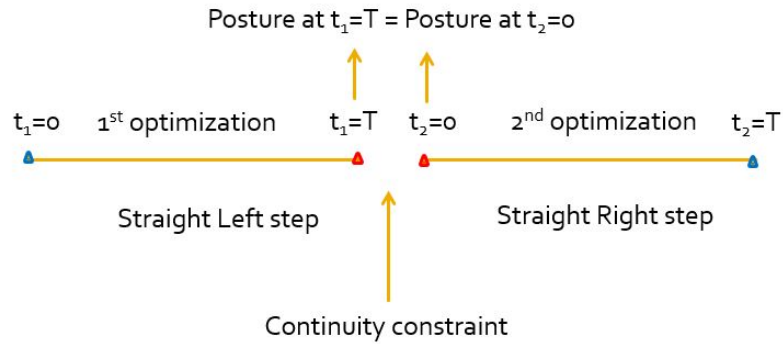


Figure 3.1 Continuity condition constraint

3.2 Results

The nonlinear optimization problem of jogging motion simulation is solved using a sequential quadratic programming (SQP) algorithm in SNOPT (Gill, Murray, and Saunders 2002). In addition to normal jogging, cause and effect studies are presented for different loading conditions (40lb and 80 lb). The left step is solved first and then its initial and final postures are used as input for the right step to solve the problem.

The optimization problem has 330 design variables (55 DOFs each with 6 control points) along with 1289 nonlinear constraints for left step and 2679 nonlinear constraints for the right step. Tracking error is minimized to get an initial kinematics solution which is used as the starting point when the other two objective functions of dynamic effort and position symmetry are added to solve the left step problem. The optimality and feasibility tolerances are both set to $\epsilon = 10^{-3}$ and the optimal solution is obtained in 585 CPU seconds for left step and 400 seconds for right step on an Intel i7, 16 GHz computer. Objective function values are 3.038 for tracking, 0.8005 for dynamic effort and 0.1735 for symmetry

objective. The results are compared with running simulation results from Chung (2009), walking simulation results from Xiang (2008), other experimental results from literature (Novacheck, 1998) and a one-step walking simulation of Santos at a velocity of 0.8 m/s and a step length of 0.5. Figure 3.2 shows slices of the motion at 0, 25, 50, 75 and 100 % of total time of motion.



Figure 3.2 Straight Jogging Left Step Motion Slices at 0, 25, 50, 75 and 100% T

3.2.1 Joint Torque Profiles

Figure 3.3 shows the joint torque profiles of hip and knee for the one-step simulation of jogging. The results compare well with running results of Chung (2009) and Novacheck (1998) as well as walking results of Xiang (2008) and show reasonable trend in general. The hip and knee torques compare well with the walking one step simulation

hip and knee torques as well. A small offset can be observed in the plots which is due to the reduced percentage of double support in the jogging motion. The hip begins to flex with the left toe strike and maximum extension torque is reached with the right foot toe strike. The knee is flexed at the start when left toe strikes but then reverses to an extension torque.

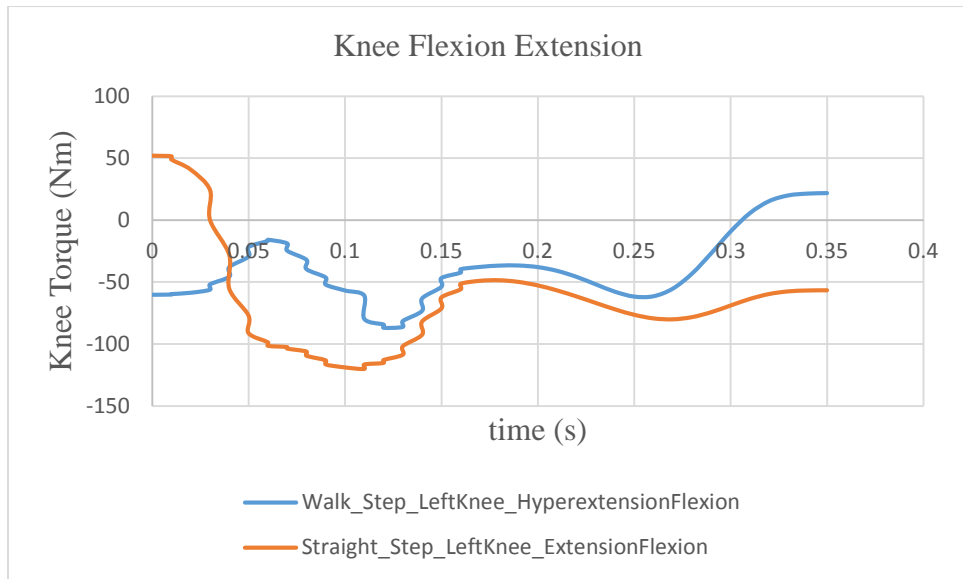
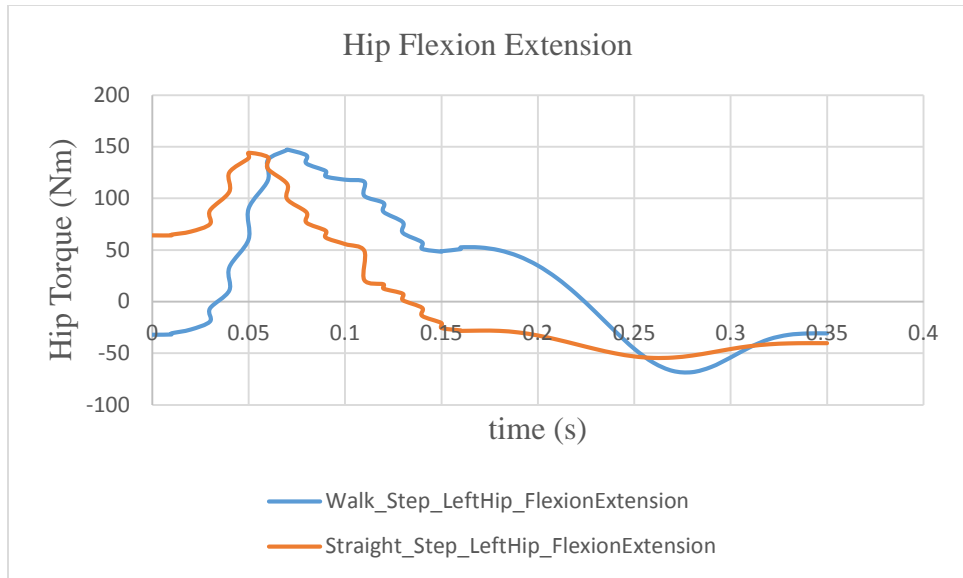


Figure 3.3: Comparison of Joint Torque Profiles for Straight Jogging Left Step and Walking Left Step Simulations

3.2.2 Ground Reaction Forces

Vertical ground reaction force (corresponding to the global y-axis) results are shown in figure 3.4. All GRFs are normalized to body weight (816.78 N). The results show a reasonable trend with the walking results. The peak force occurs after the initial toe strike and is well within the range reported by Keller (1996) and many other results from the literature. Figure 3.5 depicts the forward GRF (corresponding to the global z-axis) in the jogging direction where there is deceleration after initial toe strike and an acceleration force at push off. It differs from the walking simulation result but compares well with Chung (2009) and Xiang (2008). Figure 3.6 shows the lateral GRF (corresponding to the global x-axis) where the foot is shown to be pushing laterally during the stance phase. The lateral force shows similar trend compared to the walking result.

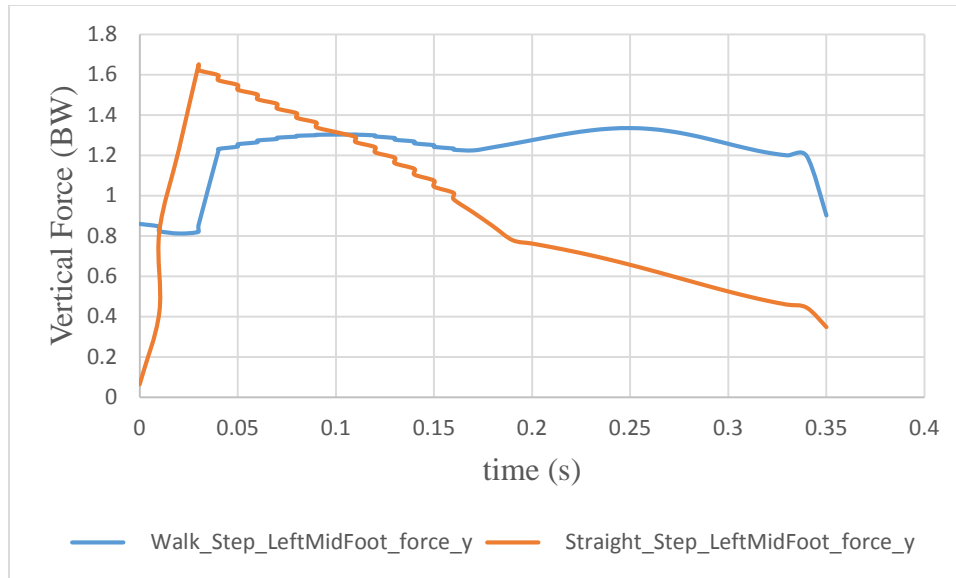


Figure 3.4: Comparison of Vertical GRF for Straight Jogging Left Step and Walking Left Step Simulations

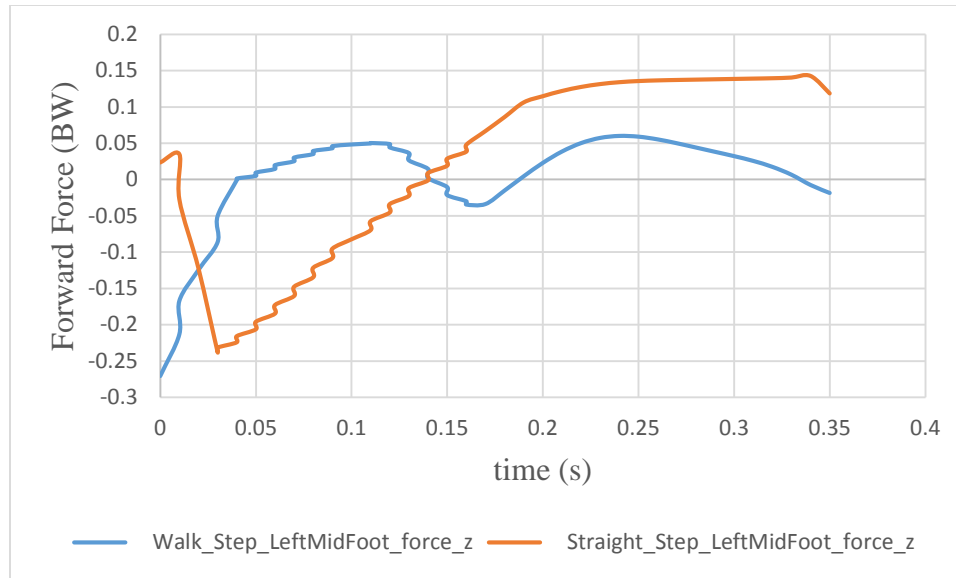


Figure 3.5: Comparison of Fore-Aft GRF for Straight Jogging Left Step and Walking Left Step Simulations

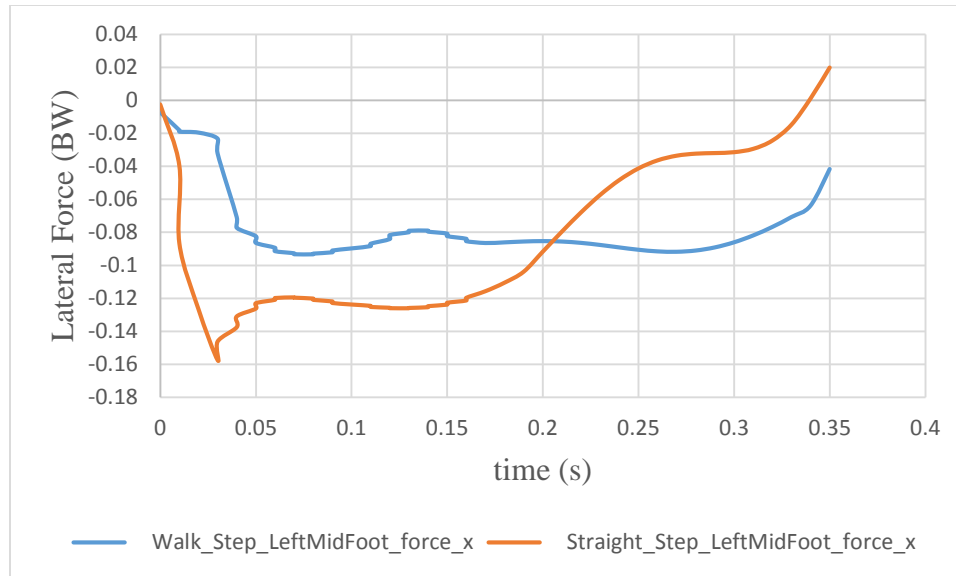


Figure 3.6: Comparison of Lateral GRF for Straight Jogging Left Step and Walking Left Step Simulations

3.2.3 Kinematics

Figure 3.7 depicts the hip and knee flexion and extension angles in radians. The results compare well with the literature (Novacheck, 1998) and show reasonable trend in general. The hip and knee joint angles compare well with the walking one step simulation hip and knee angles as well.

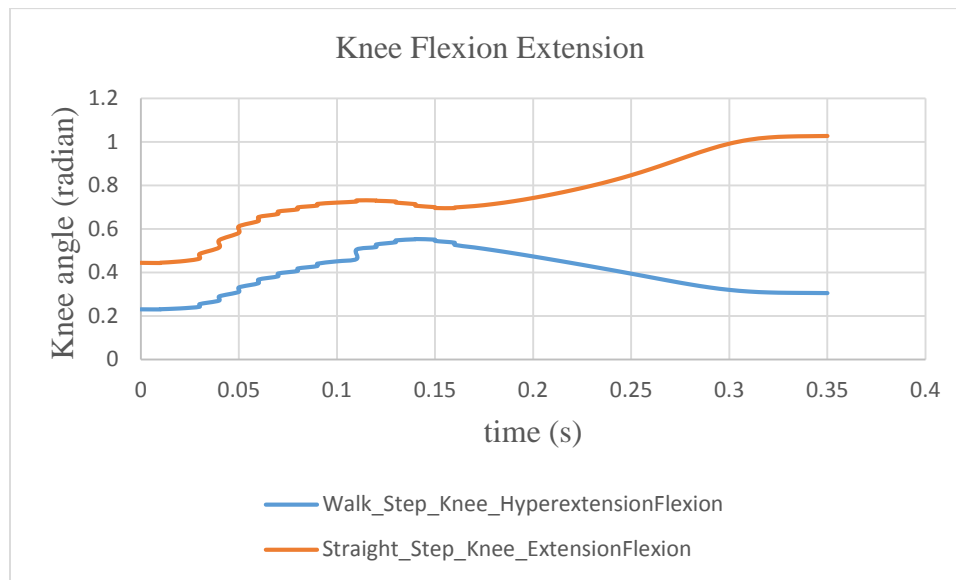
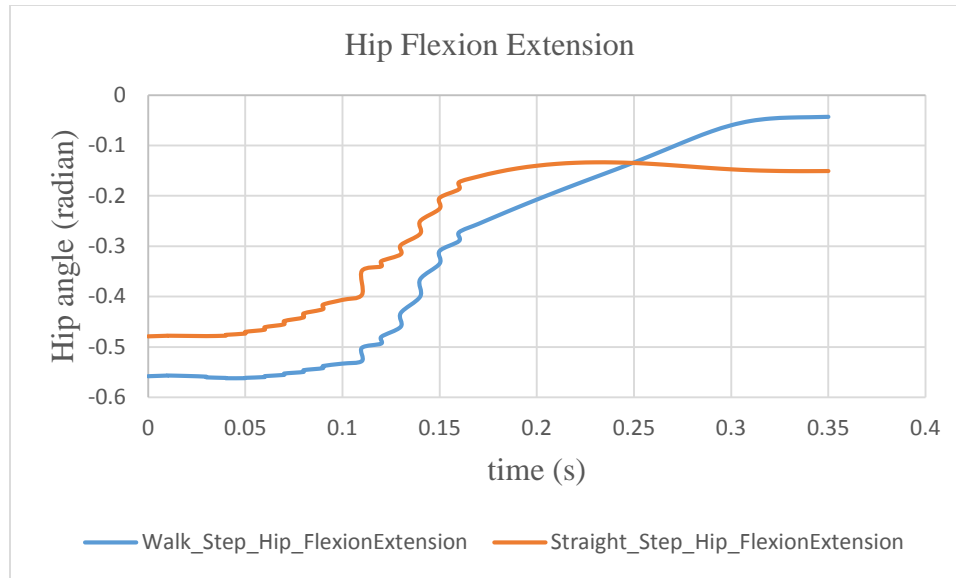


Figure 3.7: Comparison of Joint Angle Profiles for Straight Jogging Left Step and Walking Left Step Simulations

3.2.4 Cause and Effect Studies

In this section, simulation results for different loading conditions are presented. Figure 3.8 depicts the hip and knee joint torques, figures 3.9, 3.10 and 3.11 show the ground reaction force results and figure 3.12 shows joint angle profiles for three cases: no load, jogging with a 40 lb backpack and jogging with an 80 lb backpack. The 80 lb backpack case has a larger peak torque than 40 lb or no load cases. The ground reaction forces justifiably increase with increasing loads. Significant load effect is observed on the vertical GRF. For the forward force, the 80 lb backpack shows a greater minimum force compared to the 40 lb backpack. For the lateral GRF, the 80 lb backpack shows a larger peak force than the 40 lb backpack. The hip and knee joint angles do not show much change since the jogging velocity and step length is not changed. However, there is increased spine bending due to the added external load which is reflected well in the simulation results.

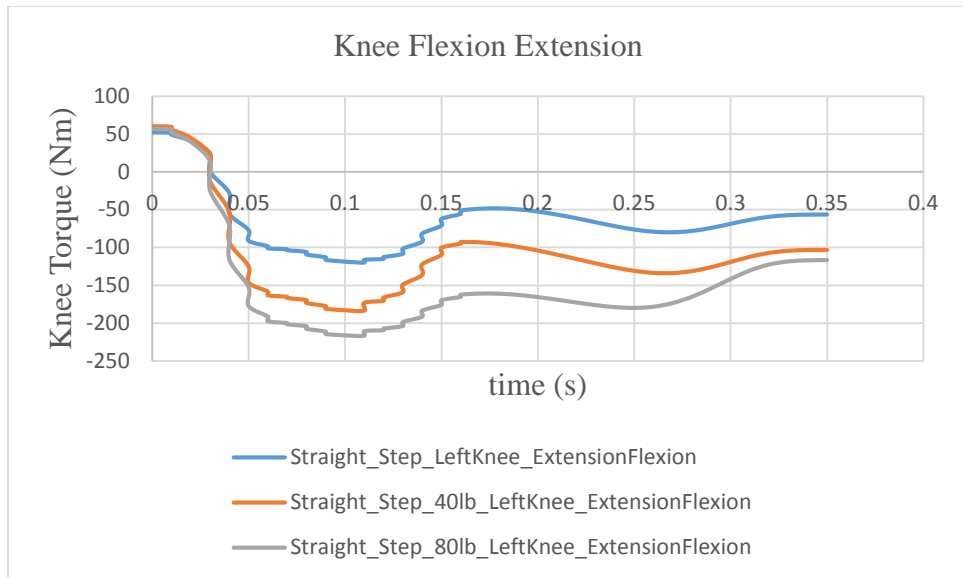
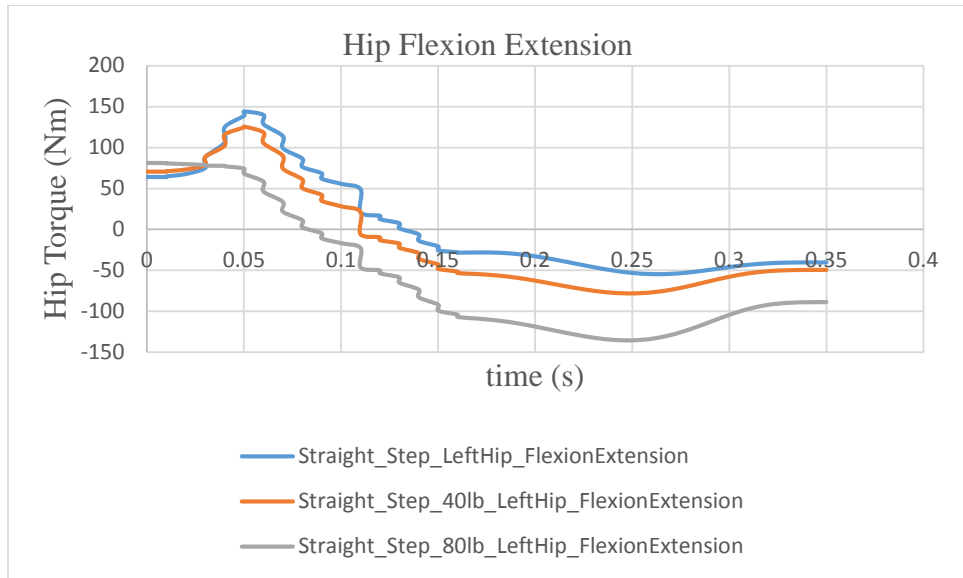


Figure 3.8: Comparison of Joint Torque Profiles for Straight Jogging Left Step

Simulations with No Load, 40 lb Backpack and 80 lb Backpack

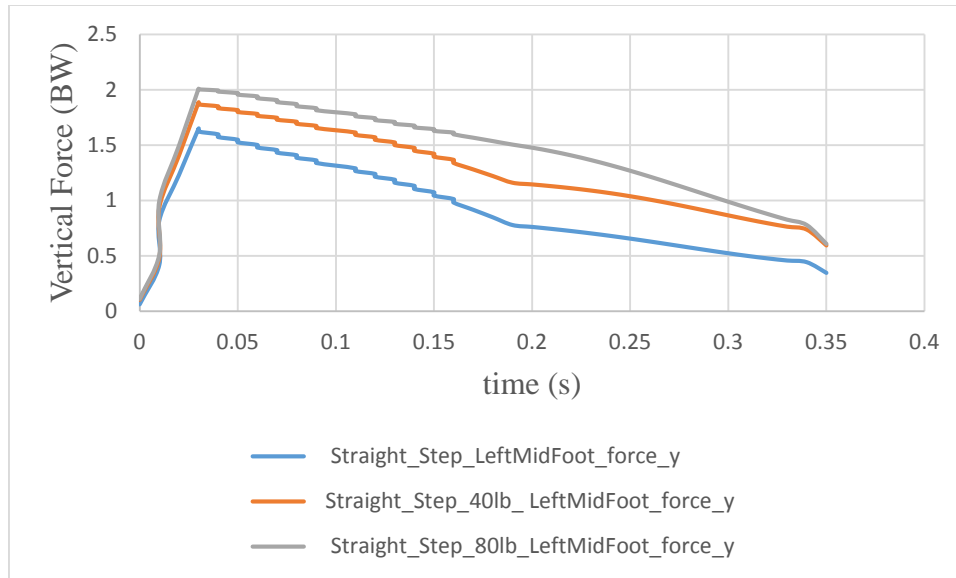


Figure 3.9: Comparison of Vertical GRF for Straight Jogging Left Step Simulations with No Load, 40 lb Backpack and 80 lb Backpack

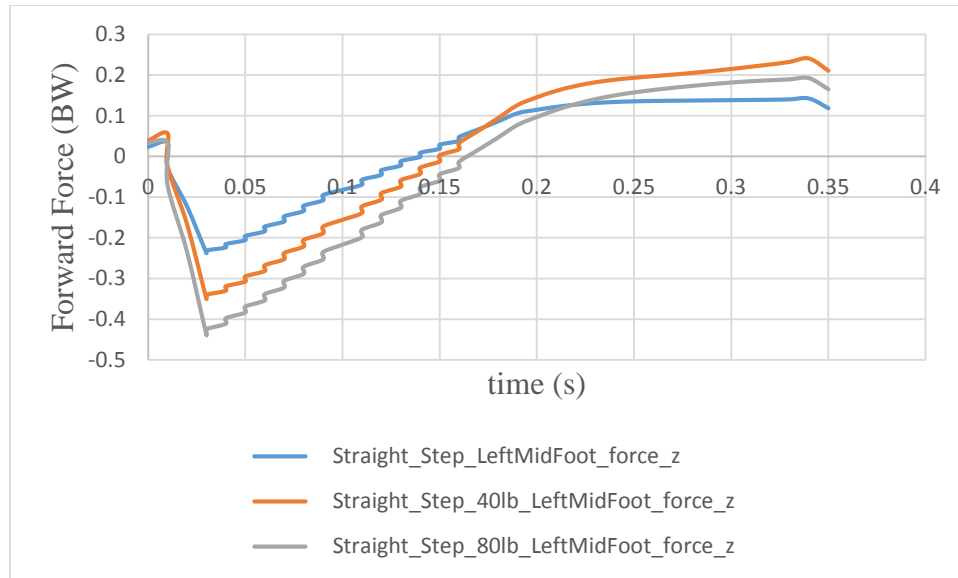


Figure 3.10: Comparison of Fore-Aft GRF for Straight Jogging Left Step Simulations with No Load, 40 lb Backpack and 80 lb Backpack

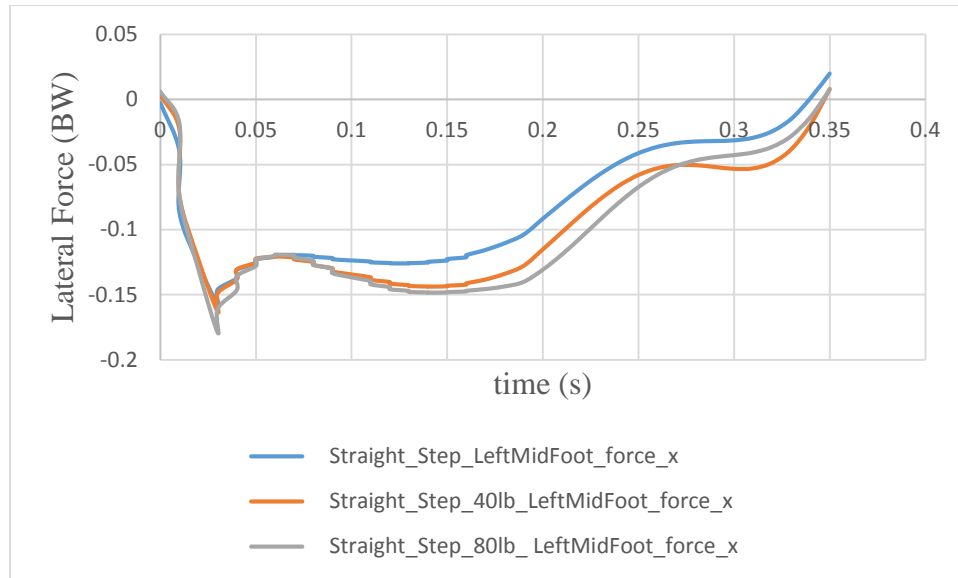
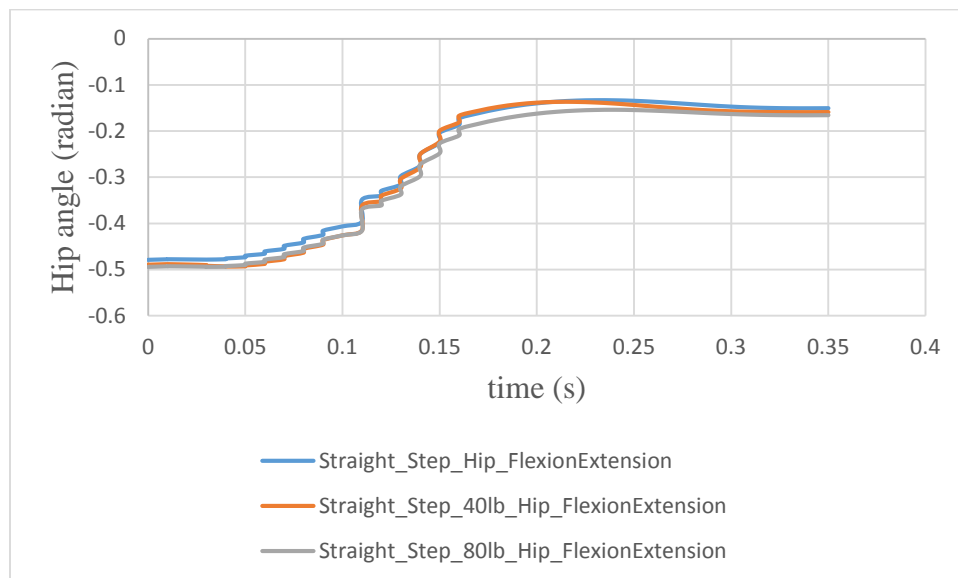


Figure 3.11: Comparison of Lateral GRF for Straight Jogging Left Step Simulations with No Load, 40 lb Backpack and 80 lb Backpack



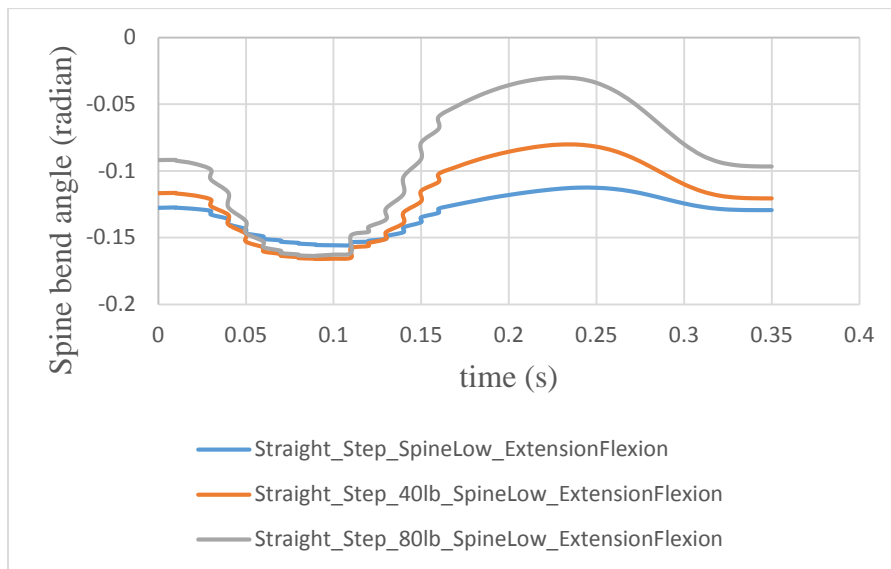
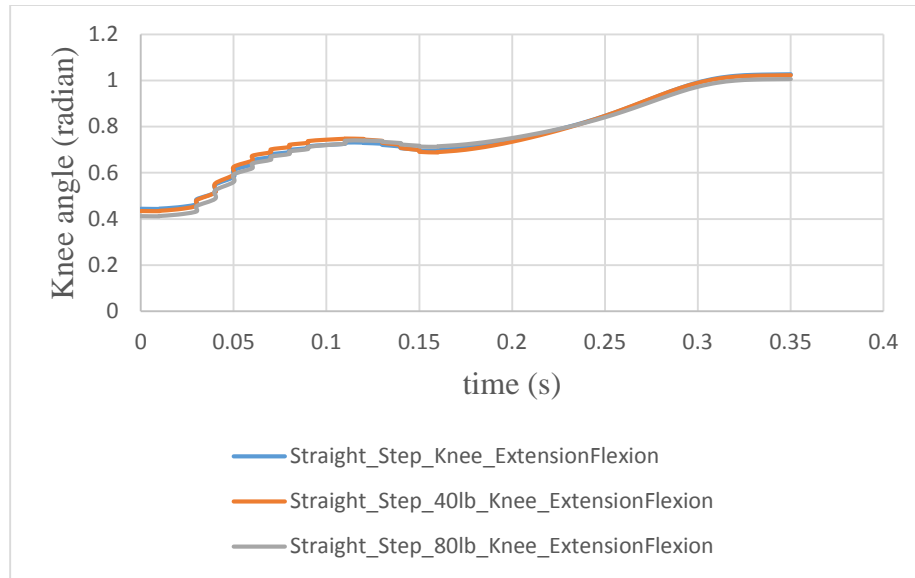


Figure 3.12: Comparison of Joint Angles for Straight Jogging Left Step Simulations with No Load, 40 lb Backpack and 80 lb Backpack

CHAPTER 4: DYNAMIC PREDICTION OF JOGGING ALONG A STRAIGHT PATH: ONE-STRIDE FORMULATION

In this chapter, normal jogging simulation along a straight path is presented using the one-stride formulation. The problem is formulated as a nonlinear optimization problem. The laws of physics are enforced by evaluating the equations of motion in the optimization process using inverse dynamics. SNOPT, a commercial software based on sequential quadratic programming (SQP) is used to solve the problem (Gill, Murray, and Saunders, 2002). Besides normal jogging, the effects of external loading are also observed. The joint torques and ground reaction forces are obtained from the simulations and studied.

4.1 Optimization Formulation

4.1.1 Task Description

The task is described as follows: Given a marker, Santos jogs towards the marker on a straight path. The stride formulation is tested for this asymmetric task where Santos carries a gun in his left hand.

4.1.2 Data Collection

A velocity of 2 m/s is used for the task. The anthropometry (height and weight) of the subject is used as an input. Based on the velocity and the subject height, the step length L is calculated according to the following equation (Bruderlin and Calvert, 1996):

$$L = 0.1394 + (0.00465 + level) * v * \sqrt{\frac{body_height}{1.8}} \text{ m} \quad (4.1)$$

where v is running speed in m/min, $level$ is the level of expertise in running ranging from -0.001 for poor to 0.001 for skilled and $body_height$ is the height of the human body (in meters). The time duration for the step is then calculated as $T=2*L/v$.

4.1.3 Optimization Design Variables

The joint angle profiles $\mathbf{q}(t)$ parameterized using B-spline approximation are used as design variables for the optimization problem.

4.1.4 Objective Function

Motion capture data has been used in this work to improve motion simulation. The difference or error between the desired joint angles from motion capture and the actual joint angles forms the first performance criterion. It is also termed as the tracking error and is minimized in the optimization formulation.

$$f_1 = \sum_{i=1}^{ndof} \int_{t=0}^T (q_{id}(t) - q_i(t))^2 dt \quad (4.2)$$

where $ndof$ is the number of DOF, q_{id} is the desired joint angle vector for the i_{th} DOF and q_i is the actual joint angle vector for the i_{th} DOF.

The time integral of the squares of all joint torques, also termed as dynamic effort, is used as the other performance criterion for the jogging motion (Fregly 2007, Xiang et al. 2010a):

$$f_2 = \sum_{i=1}^{ndof} \int_{t=0}^T \left(\frac{\tau_i}{|\tau|_{max}} \right)^2 dt \quad (4.3)$$

where $|\tau|_{\max}$ is the maximum absolute value of all the joint torque limits; $ndof$ is the number of DOF; T is the last time point, i.e., total time.

The overall objective function is a weighted combination of the two performance measures stated above.

$$f(\mathbf{P}) = (w_1 * f_1) + (w_2 * f_2) \quad (4.4)$$

where w_1 and w_2 are the weights for the objective functions. Tracking error is minimized to get an initial kinematics solution with $w_1 = 1$ and $w_2 = 0$ which is used as the starting point when dynamic effort is added with $w_1 = 0.5$ and $w_2 = 0.5$. The weights for the objective functions are selected such that $\sum w_i = 1$.

4.1.5 Constraints

Two types of constraints are considered for the jogging optimization problem as specified before: time-dependent and time-independent constraints. The time-dependent constraints include (1) joint angle limits; (2) joint torque limits; and (3) ZMP stability. These constraints are detailed as follows:

(1) Joint angle limits

The physical range of motion of joints accounts for the joint angle limits (Xiang et al. 2010a).

$$\mathbf{q}^L \leq \mathbf{q}(t) \leq \mathbf{q}^U, \quad 0 \leq t \leq T \quad (4.5)$$

(2) Joint torque limits

The dynamic physical strength of joints accounts for the joint torque limits where the maximum strength (τ_i^L or τ_i^U) of a particular joint, i , of a person changes with a change in its joint angle position $q(t)$ and velocity $\dot{q}(t)$.

$$\tau_i(q(t), \dot{q}(t))^L \leq \tau_i(t) \leq \tau_i(q(t), \dot{q}(t))^U; 0 \leq t \leq T; i = 1, \dots, ndof \quad (4.6)$$

(3) ZMP stability

The stability condition is imposed by locating ZMP position in the foot supporting region (FSR) as follows (Xiang et al. 2010a):

$$z_{ZMP}(t) \in FSR, \quad y_{ZMP}(t) \in FSR, \quad 0 \leq t \leq T \quad (4.7)$$

Time independent constraints are as follows:

(1) Foot contacting positions

Foot contacting positions during the motion are specified based on the step length L to satisfy the step length constraint. The optimization process determines the initial and final postures, velocities and accelerations.

(2) Continuity conditions

$$\begin{aligned} q_i(0) - q_i(T) &= 0, & i &= 2, 3, \dots, n \\ \dot{q}_j(0) - \dot{q}_j(T) &= 0, & j &= 1, 2, \dots, n \\ |\ddot{q}_k(0) - \ddot{q}_k(T)| &\leq \varepsilon, & k &= 1, 2, \dots, n \end{aligned} \quad (4.8)$$

where n is the number of DOFs and ε is a positive number ranging from 0.001 to 10. The position continuity constraint is excluded for the first DOF which corresponds to global translation along the jogging direction. The continuity condition file is shown in Table 4.1 where 0 refers to no symmetry, 1 refers to continuity and -1 refers to symmetry. In some cases, a smaller value for ε for the acceleration continuity constraint may result in an

infeasible solution indicating a conflict with other constraints. Hence, a large value for ϵ may be used for the constraint to account for the discontinuities resulting due to the impulse-like forces at toe-strike.

Table 4.1: Continuity File for Stride Formulation

DOF	Continuity Condition
GT1	0
GT2	1
GT3	1
GR1	1
GR2	1
GR3	1
SpineLow_LeftRightBend	1
SpineLow_ExtensionFlexion	1
SpineLow_RightLeftRotation	1
SpineMidLow_LeftRightBend	1
SpineMidLow_ExtensionFlexion	1
SpineMidLow_RightLeftRotation	1
SpineMidHigh_LeftRightBend	1
SpineMidHigh_ExtensionFlexion	1
SpineMidHigh_RightLeftRotation	1
SpineHigh_LeftRightBend	1
SpineHigh_ExtensionFlexion	1

SpineHigh_RightLeftRotation	1
RightClavicle_ElevationDepressionShrug	1
RightClavicle_RetractionProtraction	1
RightShoulder_AbductionAdduction	1
RightShoulder_ExtensionForwardFlexion	1
RightShoulder_InternalRotationExternalRotation	1
RightElbow_FlexionExtension	1
RightWrist_PronationSupination	1
RightWrist_RadialUlnarDeviation	1
RightWrist_ExtensionFlexion	1
LeftClavicle_ElevationDepressionShrug	1
LeftClavicle_RetractionProtraction	1
LeftShoulder_AbductionAdduction	1
LeftShoulder_ExtensionForwardFlexion	1
LeftShoulder_InternalRotationExternalRotation	1
LeftElbow_FlexionExtension	1
LeftWrist_PronationSupination	1
LeftWrist_RadialUlnarDeviation	1
LeftWrist_ExtensionFlexion	1
LowerNeck_LeftRightBending	1
LowerNeck_ExtensionFlexion	1
LowerNeck_RightLeftRotation	1
UpperNeck_LeftRightBending	1

UpperNeck_ExtensionFlexion	1
RightHip_AbductionAdduction	1
RightHip_FlexionExtension	1
RightHip_ExternalRotationInternalRotation	1
RightKnee_ExtensionFlexion	1
RightAnkle_DorsiPlantarFlexion	1
RightAnkle_EversionInversion	1
RightMidFootLateral_ExtensionFlexion	1
LeftHip_AbductionAdduction	1
LeftHip_FlexionExtension	1
LeftHip_ExternalRotationInternalRotation	1
LeftKnee_ExtensionFlexion	1
LeftAnkle_DorsiPlantarFlexion	1
LeftAnkle_EversionInversion	1
LeftMidFootLateral_ExtensionFlexion	1

4.2 Results

The nonlinear optimization problem of straight jogging motion simulation with one-stride formulation is solved using a sequential quadratic programming (SQP) algorithm in SNOPT (Gill, Murray, and Saunders 2002). In addition to normal jogging, cause and effect studies are presented for different loading conditions (40lb and 80 lb).

The optimization problem has 495 design variables (55 DOFs each with 9 control points) along with 1948 nonlinear constraints. Tracking error is minimized to get an initial kinematics solution which is used as the starting point when the other objective function of dynamic effort is added to solve the problem. The optimality and feasibility tolerances are both set to $\varepsilon = 10^{-3}$ and the optimal solution is obtained in 956 CPU seconds on an Intel i7, 16 GHz computer. Objective function values are 2.491 for tracking and 1.6738 for dynamic effort objective. The results are compared with running simulation results from Chung (2009), walking simulation results from Xiang (2008), other experimental results from the literature (Novacheck, 1998) and a one-stride walking simulation of Santos at a velocity of 0.8 m/s and a step length of 0.5. Figure 4.1 shows slices of the motion at 0, 25, 50, 75 and 100 % of total time of motion.



Figure 4.1 Straight Jogging Stride Motion Slices at 0, 25, 50, 75 and 100% T

4.2.1 Joint Torque Profiles

Figure 4.2 shows the joint torque profiles of hip and knee for the one-stride simulation of jogging on a straight path. The results compare well with running results of Chung (2009) and Novacheck (1998) as well as walking results of Xiang (2008) and show reasonable trend in general. The hip and knee torques compare well with the walking one stride simulation hip and knee torques as well. A small offset can be observed in the plots which is due to the reduced percentage of double support in the jogging motion. The hip begins to flex with the left toe strike and maximum extension torque is reached with the right foot toe strike. The knee is flexed at the start when left toe strikes but then reverses to an extension torque.

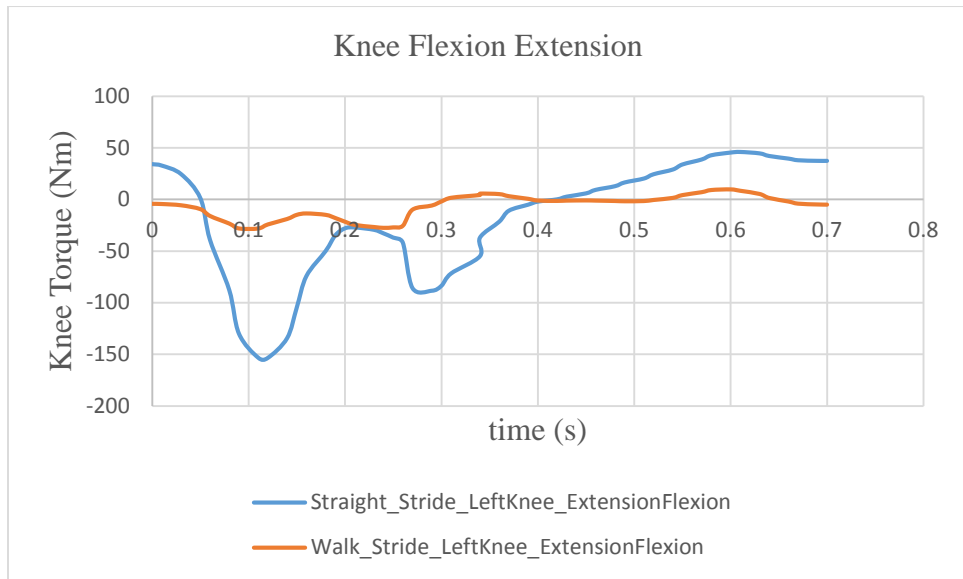
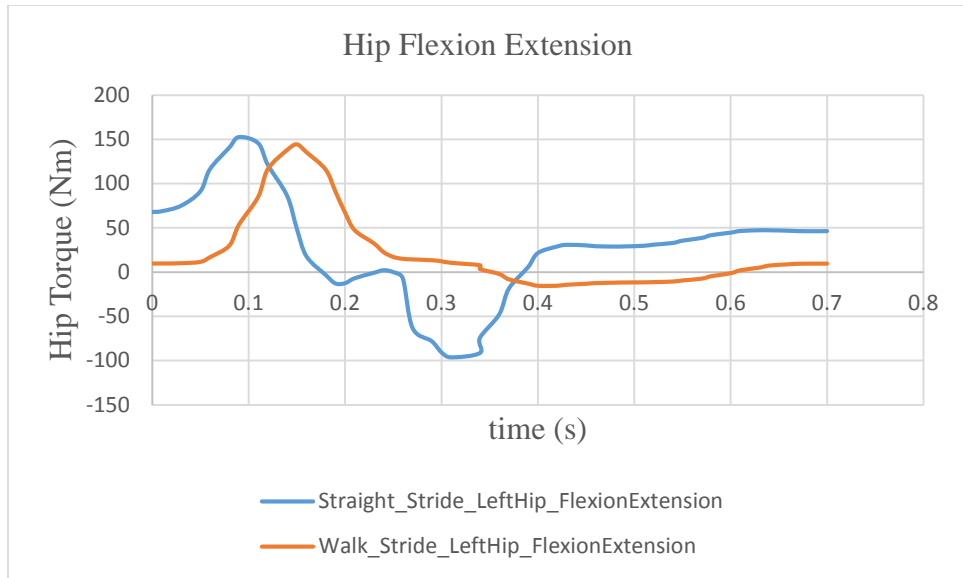


Figure 4.2: Comparison of Joint Torque Profiles for Straight Jogging Stride and Walking Stride Simulations

4.2.2 Ground Reaction Forces

Vertical ground reaction force (corresponding to the global y-axis) results are shown in figure 4.3. All GRFs are normalized to body weight (816.78 N). The results show a reasonable trend with the walking results. The peak force occurs after the initial toe strike and is well within the range reported by Ounpuu (1994) and Novacheck (1998). Figure 4.4 depicts the forward GRF (corresponding to the global z-axis) in the jogging direction where there is deceleration after initial toe strike and an acceleration force at push off. It differs from the walking simulation result but compares well with Chung (2009) and Xiang (2008). Figure 4.5 shows the lateral GRF (corresponding to the global x-axis) where the foot is shown to be pushing laterally during the stance phase. It shows similar trend compared to the walking result.

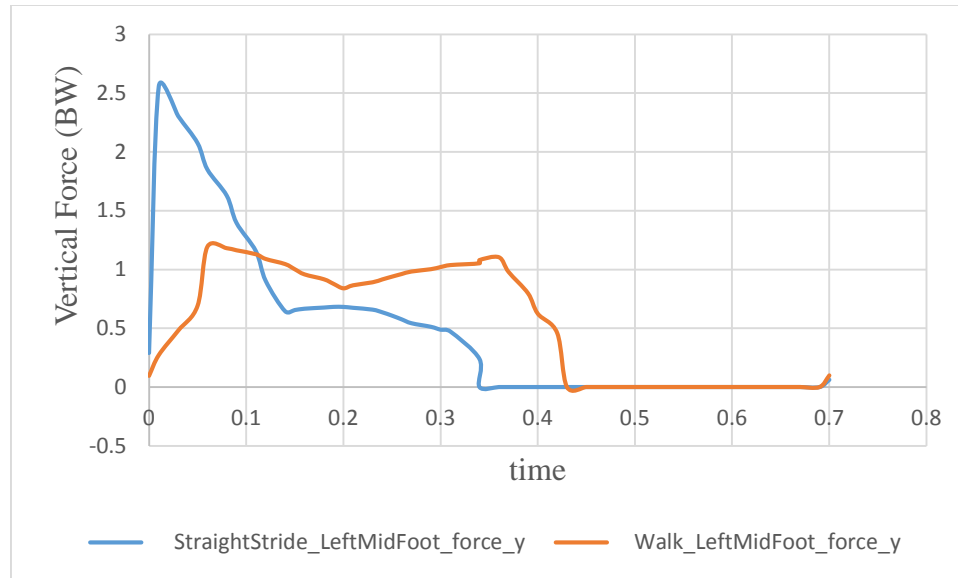


Figure 4.3: Comparison of Vertical GRF for Straight Jogging Stride and Walking Stride Simulations

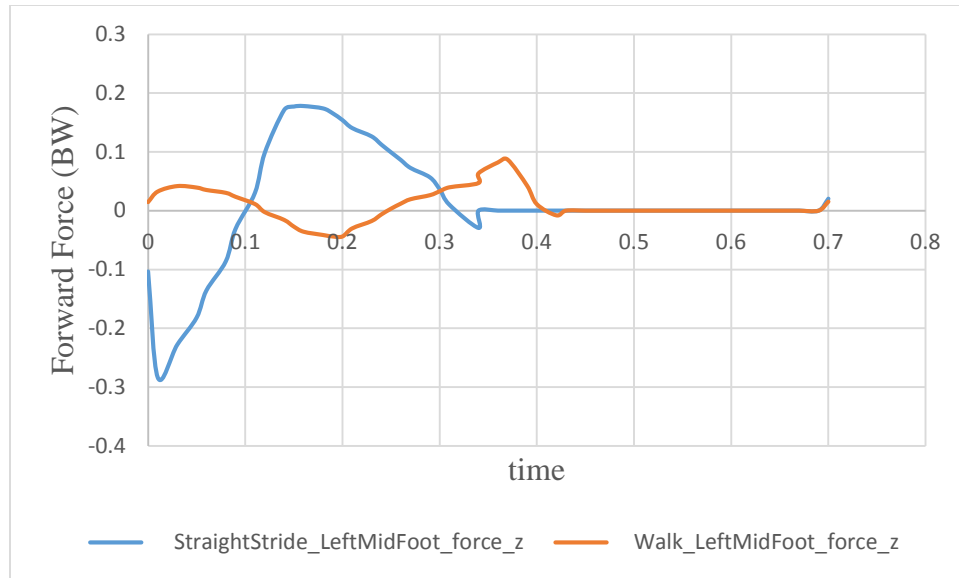


Figure 4.4: Comparison of Fore-Aft GRF for Straight Jogging Stride and Walking Stride Simulations

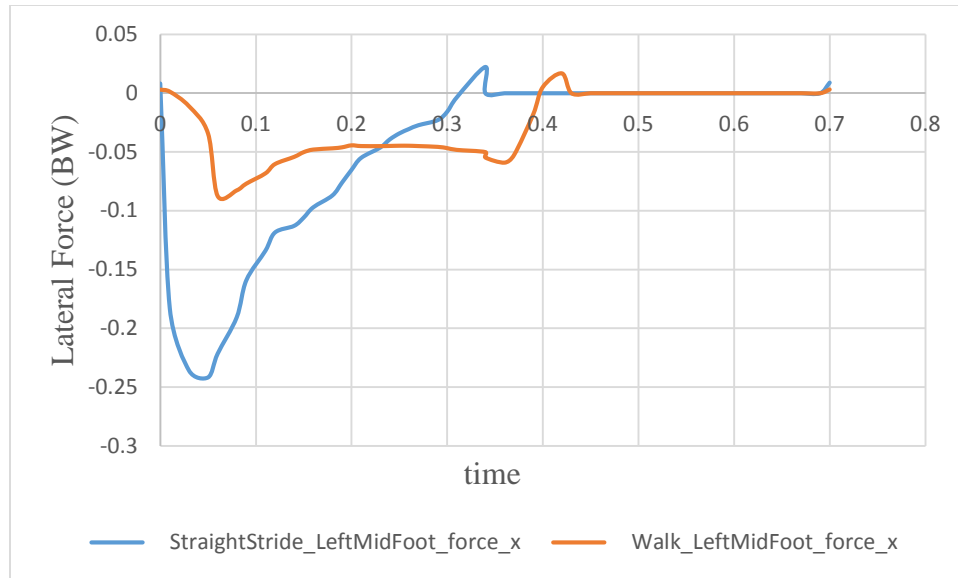


Figure 4.5: Comparison of Lateral GRF for Straight Jogging Stride and Walking Stride Simulations

4.2.3 Kinematics

Figure 4.6 depicts the hip and knee flexion and extension angles in radians. The results compare well with the literature (Novacheck, 1998) and show reasonable trend in general. The hip and knee joint angles compare well with the walking one step simulation hip and knee angles as well.

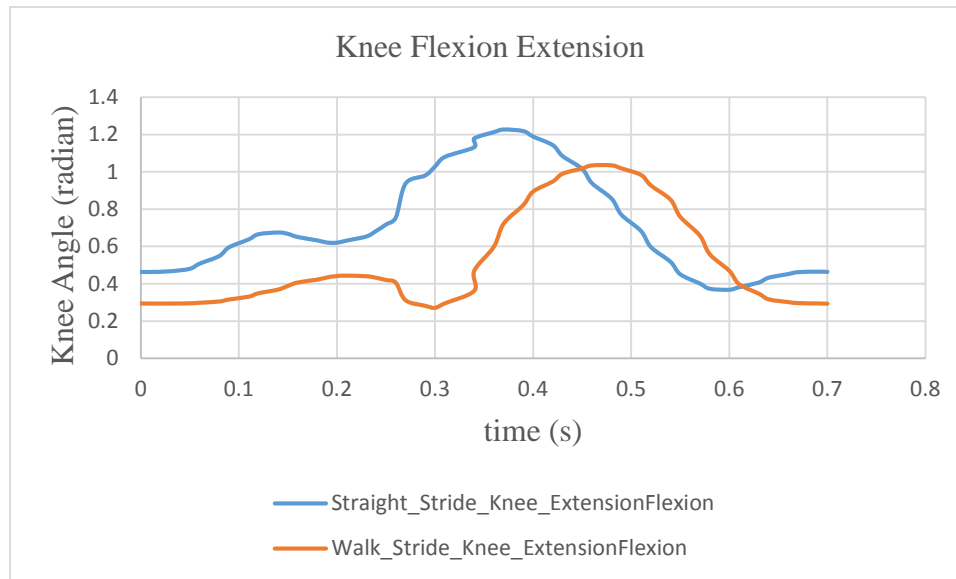
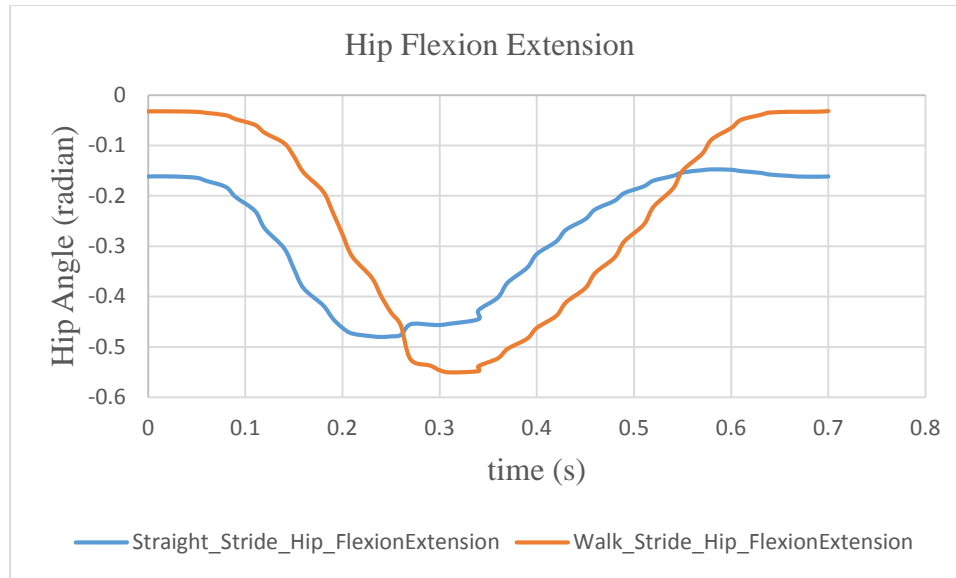


Figure 4.6: Comparison of Joint Angle Profiles for Straight Jogging Stride and Walking Stride Simulations

4.2.4 Cause and Effect Studies

In this section, simulation results for different loading conditions are presented. Figure 4.7 depicts the hip and knee joint torques, figures 4.8, 4.9 and 4.10 show the ground reaction force results and figure 4.11 shows joint angle profiles for three cases: no load, jogging with a 40 lb backpack and jogging with an 80 lb backpack. The 80 lb backpack case has a larger peak torque than 40 lb or no load cases. The ground reaction forces justifiably increase with increasing loads. Significant load effect is observed on the vertical GRF. For the forward force, the 80 lb backpack shows a greater minimum force compared to the 40 lb backpack. For the lateral GRF, the 80 lb backpack shows a larger peak force than the 40 lb backpack. The hip and knee joint angles do not show much change since the jogging velocity and step length is not changed. However, there is increased spine bending due to the added external load which is reflected well in the simulation results.

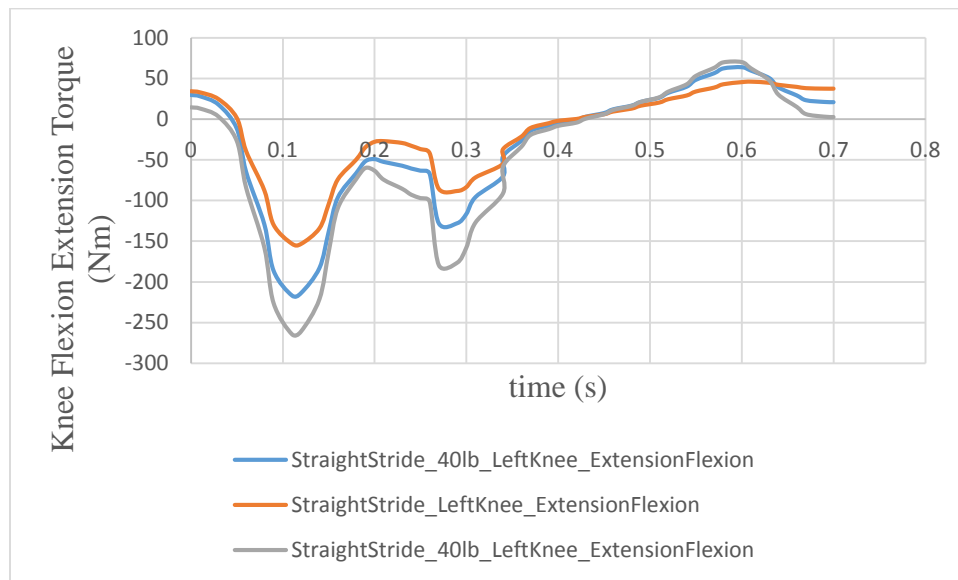
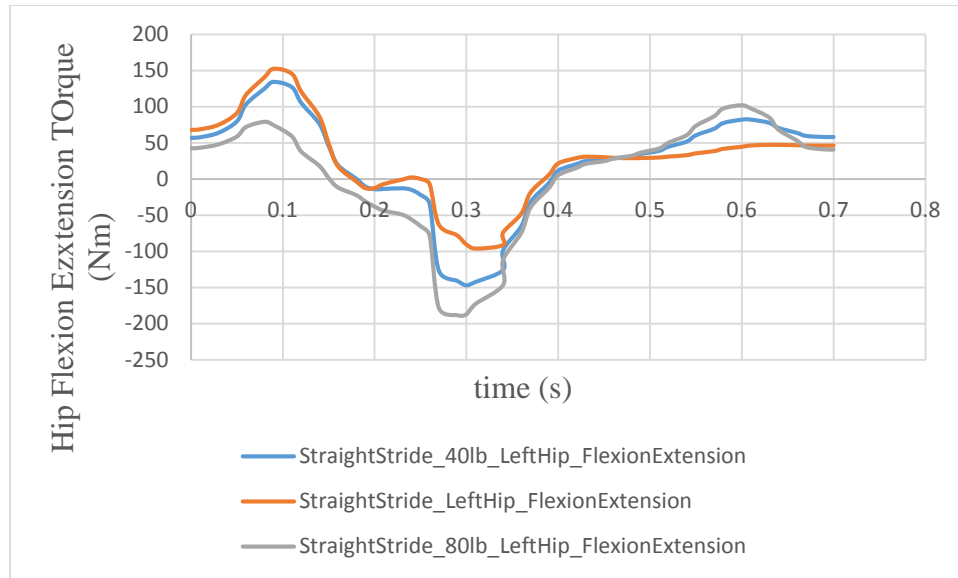


Figure 4.7 Comparison of Joint Torque Profiles for Straight Jogging Stride Simulations with No Load, 40 lb Backpack and 80 lb Backpack

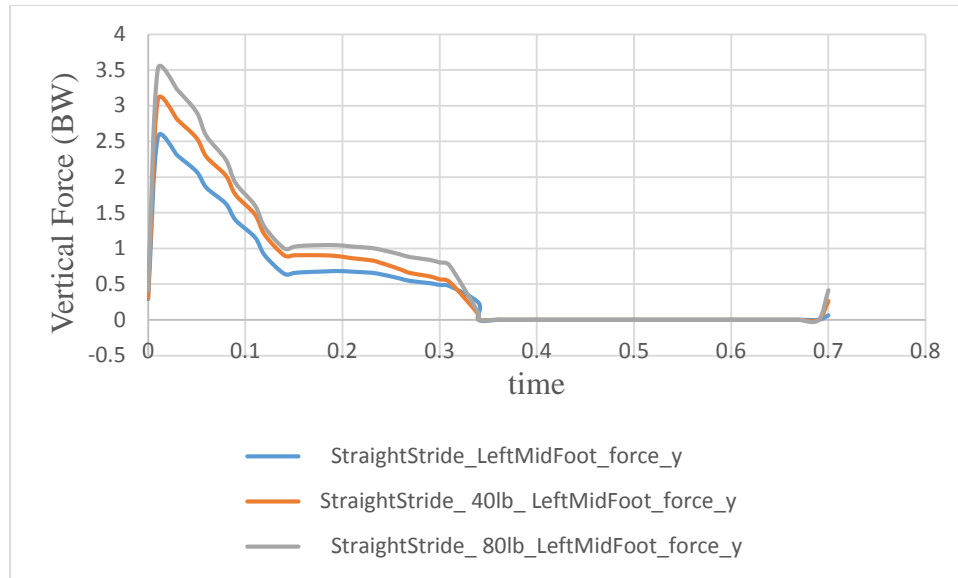


Figure 4.8 Comparison of Vertical GRF for Straight Jogging Stride Simulations with No Load, 40 lb Backpack and 80 lb Backpack

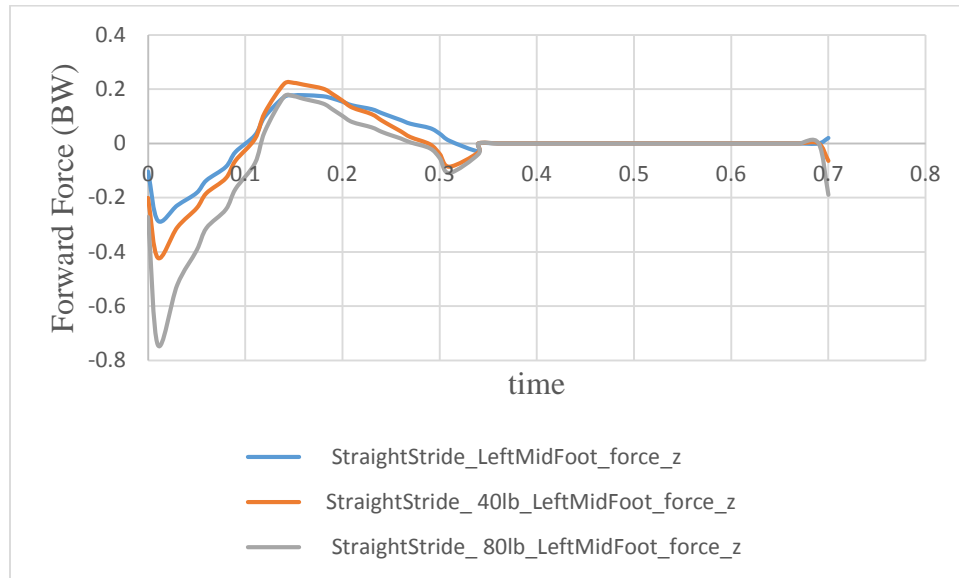


Figure 4.9 Comparison of Fore-Aft GRF for Straight Jogging Stride Simulations with No Load, 40 lb Backpack and 80 lb Backpack

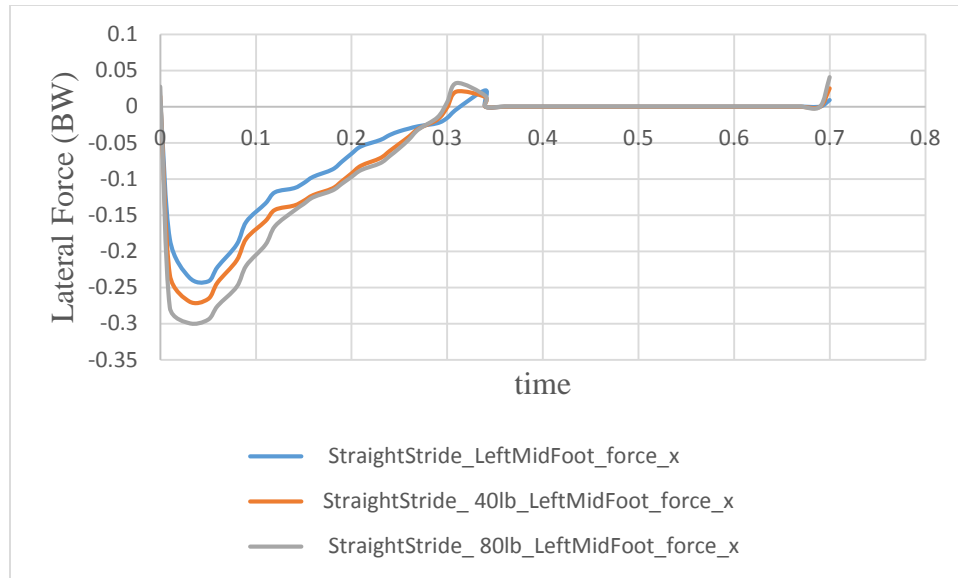
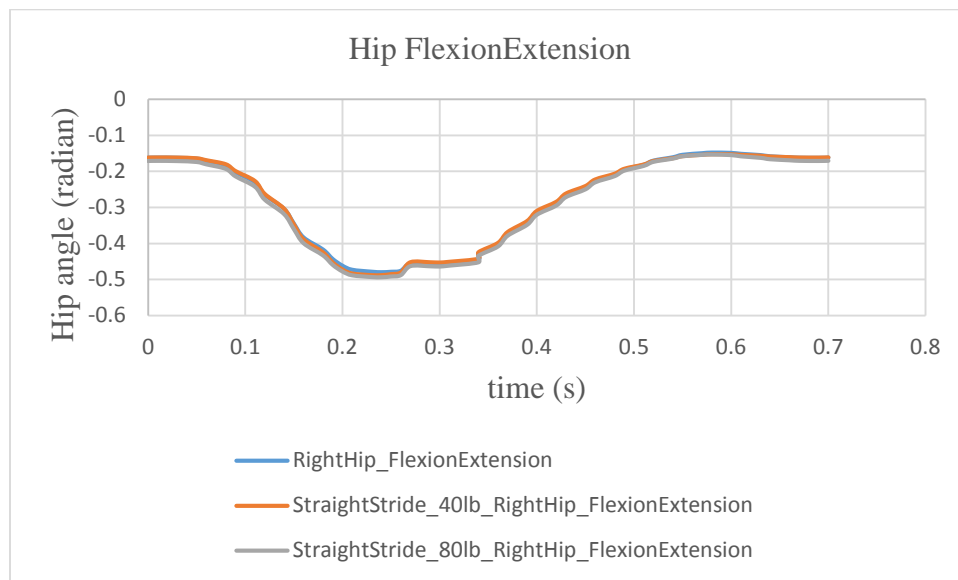


Figure 4.10 Comparison of Lateral GRF for Straight Jogging Stride Simulations with No Load, 40 lb Backpack and 80 lb Backpack



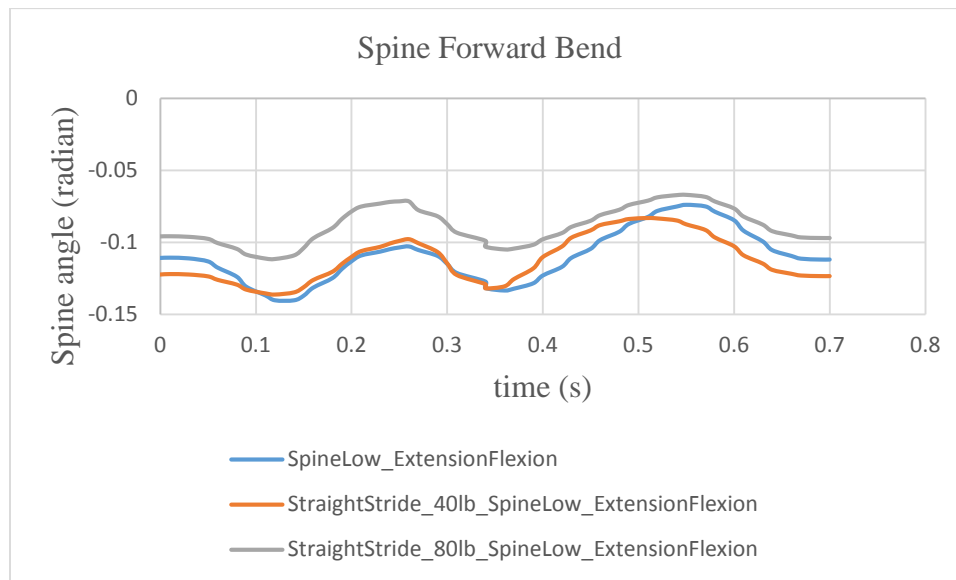
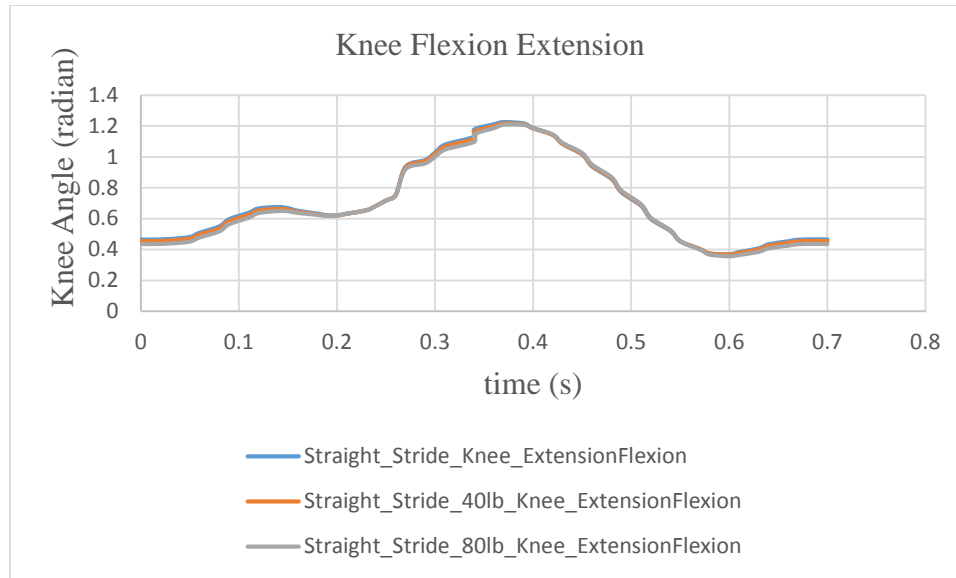


Figure 4.11 Comparison of Joint Angles for Straight Jogging Stride Simulations with No Load, 40 lb Backpack and 80 lb Backpack

4.2.5 Walking with Increased Velocity

In this section, visual results for walking stride simulation with increased double support phase and heel strike for a velocity of $v = 2$ m/s and a step length of $L = 0.5$ m are presented to test the hypothesis that simulation of human jogging by formulating the motion as a separate problem with different gait cycle phases and foot striking patterns as compared to walking provides more realistic motion. Figure 4.12 shows slices of the walking stride motion with increased velocity at 0, 25, 50, 75 and 100 % of total time of the motion.

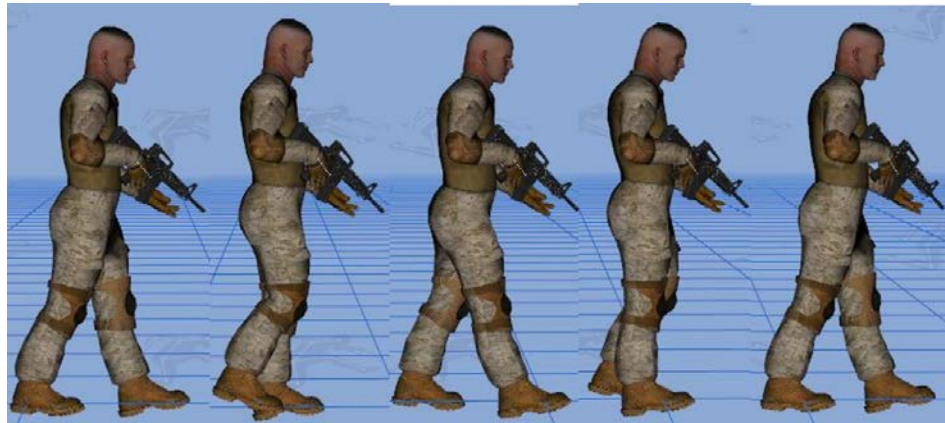


Figure 4.12 Walking Stride Simulation with Velocity 2 m/s and Step Length 0.5 m

Motion Slices at 0, 25, 50, 75 and 100% T

It is observed that the walking motion with increased velocity does not look natural and the formulation needs to be modified for realistic motion, thus proving the hypothesis that a separate jogging formulation provides more realistic results.

CHAPTER 5: DYNAMIC PREDICTION OF JOGGING ALONG A CURVED PATH: ONE-STRIDE FORMULATION

In this chapter, normal clock-wise and a counter clock-wise jogging simulation along a curve is presented using the one-stride formulation. The problem is formulated as a nonlinear optimization problem. The laws of physics are enforced by evaluating the equations of motion in the optimization process using inverse dynamics. SNOPT, a commercial software based on sequential quadratic programming (SQP) is used to solve the problem (Gill, Murray, and Saunders, 2002). Besides normal jogging, the effects of external loading are also observed. The joint torques and ground reaction forces are obtained from the simulations and studied.

5.1 Clock-wise Jogging

In this section, formulation and simulation results for clock-wise jogging along a curve are presented.

5.1.1 Optimization Formulation

5.1.1.1 Task Description

The task is described as follows: Given a marker, Santos jogs around the marker. The stride formulation is tested for this asymmetric task where motion of the left and right parts of the body is not the same and Santos carries a gun in his left hand.

5.1.1.2 Data Collection

A velocity of 2 m/s, an initial step length $L = 0.55$ m and a radius of curved path $R = 1.5$ m is used for the task. Step length L and curve radius R are used to calculate actual foot locations along the curve for the foot contact position constraint (Chung, 2009). The heel, mid-foot or the toe can be constrained on the foot to impose the foot contact position constraint.

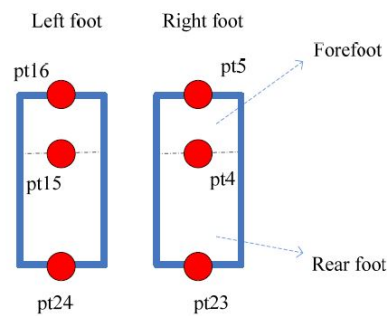


Figure 5.1 Points on the foot for foot contact position constraint

Here pt16 is left toe center, pt15 is left mid-foot center, pt24 is left heel center, pt23 is right heel center, pt4 is right mid-foot center and pt5 is right toe center.

The step length and orientation of the foot in the inertial frame of reference is required to calculate the contact location of any of these three points. Figure 5.2 describes the foot location along the curve:

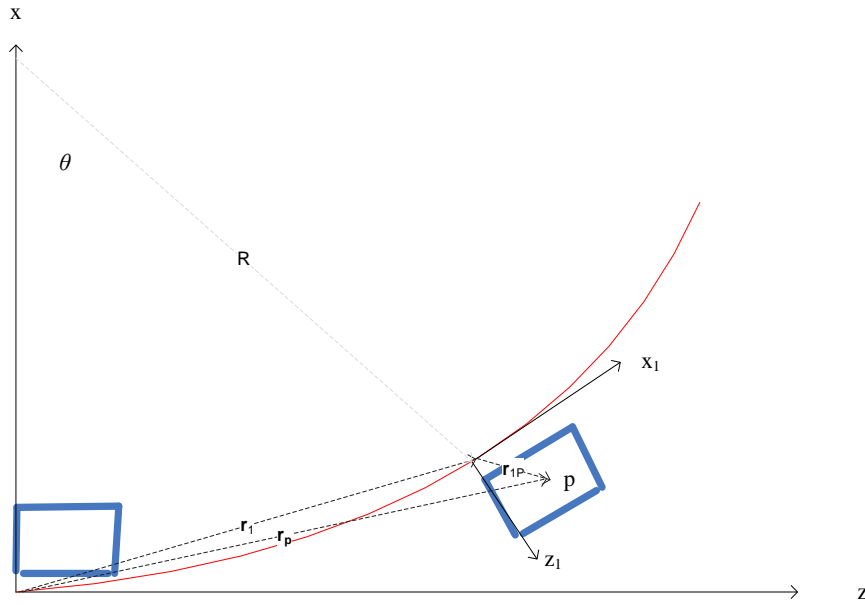


Figure 5.2 Foot location along the curve

The blue box describes the foot on the ground. The local reference frame for the foot is given by x_1-z_1 and the inertial reference frame is given by $x-z$. r_p is the vector from the origin of the inertial reference frame to the foot point p , which will be controlled in the local reference frame. r_1 is the vector from the origin of the inertial reference frame to the origin of the local reference frame. r_{1p} is the vector from the origin of the local reference frame to the foot point p in the local reference frame. What we need is r_p since the foot location constraint is applied in the inertial reference frame. The vector r_1 is given by the step length.

$$\|r_1\| = L \tag{5.1}$$

The foot orientation angle θ is calculated as follows:

$$\theta = 2 \sin^{-1} \left(\frac{L}{2R} \right) \quad (5.2)$$

The the vector of point P can be written as:

$$\mathbf{r}_p = \mathbf{r}_i + \mathbf{A}_1 \mathbf{r}_{1p} \quad (5.3)$$

$$\mathbf{r}_p = \begin{bmatrix} 2R \sin(\theta/2) \cos(\theta/2) + z_{1p} \cos \theta - x_{1p} \sin \theta \\ 2R \sin(\theta/2) \sin(\theta/2) + z_{1p} \sin \theta + x_{1p} \cos \theta \end{bmatrix} \quad (5.4)$$

where \mathbf{A}_1 is the rotation matrix of the local reference frame. For the given values of step length L and radius R, the foot orientation angle θ is approximately 30 degrees and the distance covered in one stride is 1.6 m at a velocity of 2 m/s. The time duration for the stride is then calculated as $T=1.6/2 = 0.8s$.

5.1.1.3 Optimization Design Variables

The joint angle profiles $\mathbf{q}(t)$ parameterized using B-spline approximation are used as design variables for the optimization problem.

5.1.1.4 Objective Function

Motion capture data has been used in this work to improve motion simulation. The difference or error between the desired joint angles from motion capture and the actual joint angles forms the first performance criterion. It is also termed as the tracking error and is minimized in the optimization formulation.

$$f_1 = \sum_{i=1}^{ndof} \int_{t=0}^T (q_{id}(t) - q_i(t))^2 dt \quad (5.5)$$

where $ndof$ is the number of DOF, q_{id} is the desired joint angle vector for the i_{th} DOF and q_i is the actual joint angle vector for the i_{th} DOF.

The time integral of the squares of all joint torques, also termed as dynamic effort, is used as the other performance criterion for the jogging motion (Fregly 2007, Xiang et al. 2010a):

$$f_2 = \sum_{i=1}^{ndof} \int_{t=0}^T \left(\frac{\tau_i}{|\tau|_{max}} \right)^2 dt \quad (5.6)$$

where $|\tau|_{max}$ is the maximum absolute value of all the joint torque limits; *ndof* is the number of DOF; T is the last time point, i.e., total time.

The overall objective function is a weighted combination of the two performance measures stated above.

$$f(\mathbf{P}) = (w_1 * f_1) + (w_2 * f_2) \quad (5.7)$$

where w_1 and w_2 are the weights for the objective functions. Tracking error is minimized to get an initial kinematics solution with $w_1 = 1$ and $w_2 = 0$ which is used as the starting point when dynamic effort is added with $w_1 = 0.5$ and $w_2 = 0.5$. The weights for the objective functions are selected such that $\sum w_i = 1$.

5.1.1.5 Constraints

Two types of constraints are considered for the jogging optimization problem as specified before: time-dependent and time-independent constraints. The time-dependent constraints include (1) joint angle limits; (2) joint torque limits; and (3) ZMP stability. These constraints are detailed as follows:

(1) Joint angle limits

The physical range of motion of joints accounts for the joint angle limits (Xiang et al. 2010a).

$$\mathbf{q}^L \leq \mathbf{q}(t) \leq \mathbf{q}^U, \quad 0 \leq t \leq T \quad (5.8)$$

(2) Joint torque limits

The dynamic physical strength of joints accounts for the joint torque limits where the maximum strength (τ_i^L or τ_i^U) of a particular joint, i , of a person changes with a change in its joint angle position $q(t)$ and velocity $\dot{q}(t)$.

$$\tau_i(q(t), \dot{q}(t))^L \leq \tau_i(t) \leq \tau_i(q(t), \dot{q}(t))^U; \quad 0 \leq t \leq T; \quad i = 1, \dots, ndof \quad (5.9)$$

(3) ZMP stability

The stability condition is imposed by locating ZMP position in the foot supporting region (FSR) as follows (Xiang et al. 2010a):

$$z_{ZMP}(t) \in FSR, \quad y_{ZMP}(t) \in FSR, \quad 0 \leq t \leq T \quad (5.10)$$

Time independent constraints are as follows:

(1) Foot contacting positions

Foot contacting positions during the motion are specified based on the step length L to satisfy the step length constraint. The optimization process determines the initial and final postures, velocities and accelerations.

(2) Continuity conditions

$$\begin{aligned} q_i(0) - q_i(T) &= 0, & i &= 2, 3, \dots, n \\ \dot{q}_j(0) - \dot{q}_j(T) &= 0, & j &= 1, 2, \dots, n \\ |\ddot{q}_k(0) - \ddot{q}_k(T)| &\leq \varepsilon, & k &= 1, 2, \dots, n \end{aligned} \quad (5.11)$$

where n is the number of DOFs and ϵ is a positive number ranging from 0.001 to 10. The position continuity constraint is excluded for the first DOF which corresponds to global translation along the jogging direction. The continuity condition file is shown in Table 4.1 where 0 refers to no symmetry, 1 refers to continuity and -1 refers to symmetry. In some cases, a smaller value for ϵ for the acceleration continuity constraint may result in an infeasible solution indicating a conflict with other constraints. Hence, a large value for ϵ may be used for the constraint to account for the discontinuities resulting due to the impulse-like forces at toe-strike.

5.1.2 Results

The nonlinear optimization problem of clock-wise (CW) jogging motion simulation with one-stride formulation is solved using a sequential quadratic programming (SQP) algorithm in SNOPT (Gill, Murray, and Saunders 2002). In addition to normal CW jogging, cause and effect studies are presented for different loading conditions (40lb and 80 lb).

The optimization problem has 495 design variables (55 DOFs each with 9 control points) along with 1929 nonlinear constraints. Tracking error is minimized to get an initial kinematics solution which is used as the starting point when the other objective function of dynamic effort is added to solve the problem. The optimality and feasibility tolerances are both set to $\epsilon = 10^{-3}$ and the optimal solution is obtained in 688 CPU seconds on an Intel i7, 16 GHz computer. Objective function values are 2.77 for tracking and 1.776 for dynamic effort objective. The results are compared with running simulation results from Chung (2009), other experiment results from literature (Novacheck, 1998) and the one-stride straight jogging simulation of Santos presented in chapter 4. Figure 5.3 shows slices of the motion at 0, 25, 50, 75 and 100 % of total time of motion.



Figure 5.3 CW Jogging Stride Motion Slices at 0, 25, 50, 75 and 100% T

5.1.2.1 Joint Torque Profiles

Figure 5.4 shows the joint torque profiles of hip and knee for the one-stride simulation of CW jogging on a curved path. The results compare well with running results of Chung (2009) and Novacheck (1998) and the straight stride results and show reasonable trend in general. The hip begins to flex with the left toe strike and maximum extension torque is reached with the right foot toe strike. The knee is flexed at the start when left toe strikes but then reverses to an extension torque.

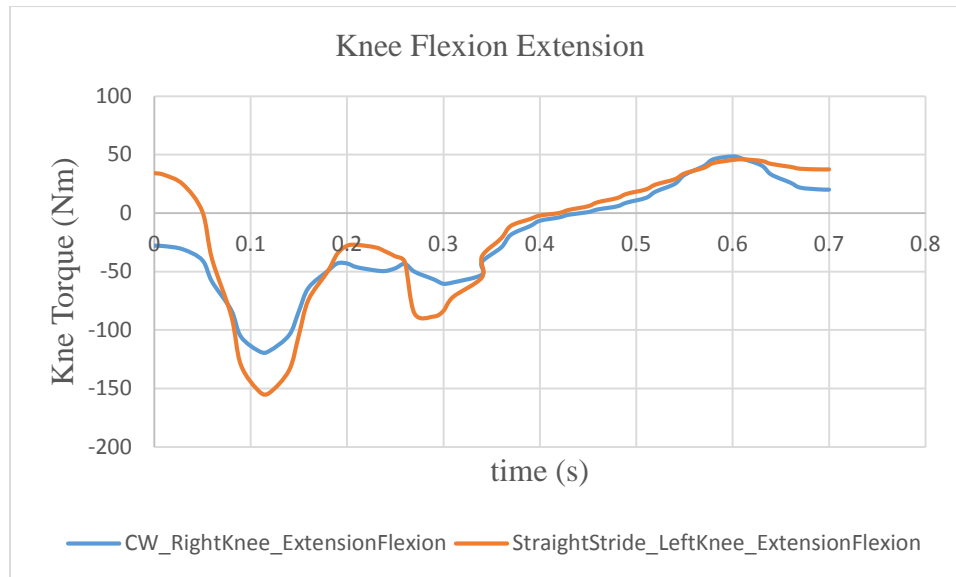
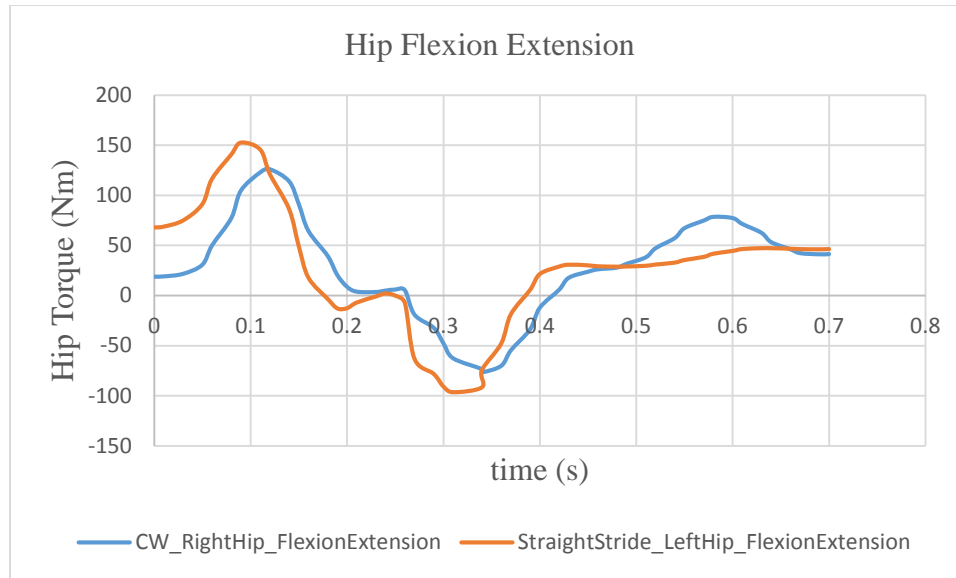


Figure 5.4: Comparison of Joint Torque Profiles for Straight Jogging Stride and Clock-wise Jogging Stride Simulations

5.1.2.2 Ground Reaction Forces

Vertical ground reaction force (corresponding to the global y-axis) results are shown in figure 5.5. All GRFs are normalized to body weight (816.78 N). The results show a reasonable trend with the straight stride results and walking results. The peak force is well within the range reported by Keller (1996). It is interesting to note that jogging along a curved path experiences lesser vertical forces and increased lateral forces as compared to straight jogging. Figure 5.6 depicts the forward GRF (corresponding to the global z-axis) and figure 5.7 shows the lateral GRF (corresponding to the global x-axis). The forward GRF compares well with Chung (2009) and Xiang (2008) as well as the straight stride results. The lateral force is justifiably higher for jogging on a curved path compared to the straight stride results as it provides the required centripetal force for the circular jog and shows reasonable trend with Chung (2009).

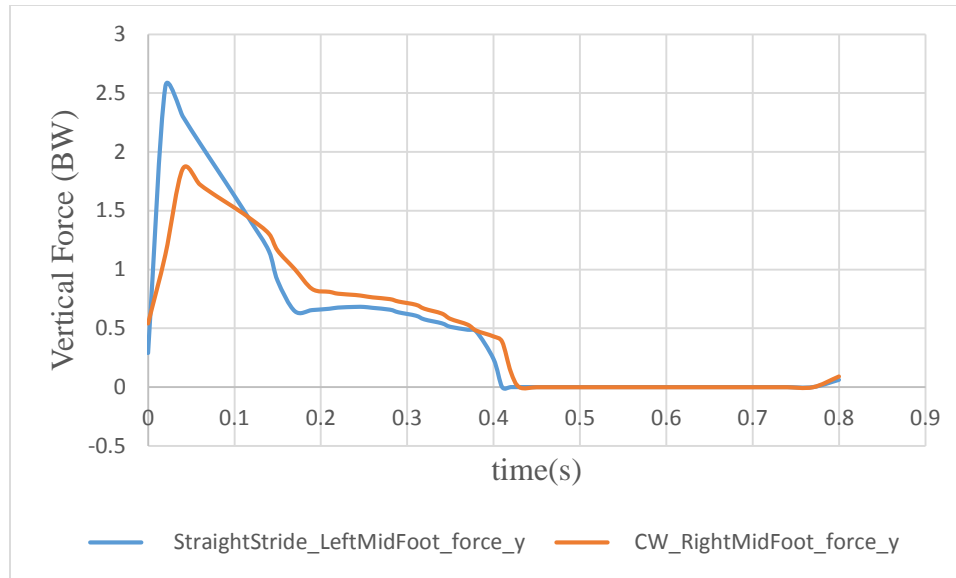


Figure 5.5: Comparison of Vertical GRF for Straight Jogging Stride and Clock-wise Jogging Stride Simulations

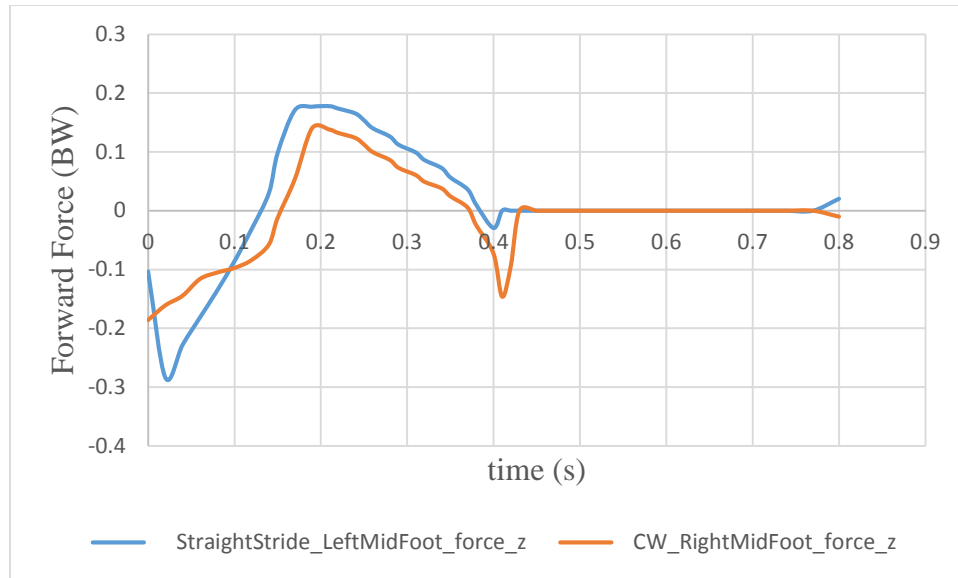


Figure 5.6: Comparison of Fire-Aft GRF for Straight Jogging Stride and Clock-wise Jogging Stride Simulations

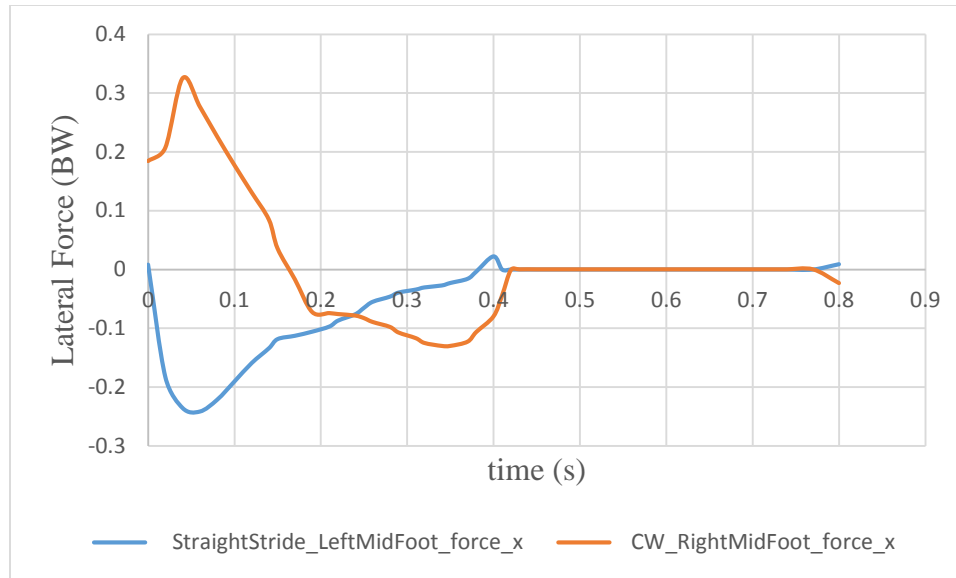


Figure 5.7: Comparison of Lateral GRF for Straight Jogging Stride and Clock-wise Jogging Stride Simulations

5.1.2.3 Kinematics

Figure 5.8 depicts the hip and knee flexion and extension angles in radians. The results compare well with the literature (Novacheck, 1998) and show reasonable trend in general. The hip and knee joint angles compare well with the jogging one stride simulation hip and knee angles as well.

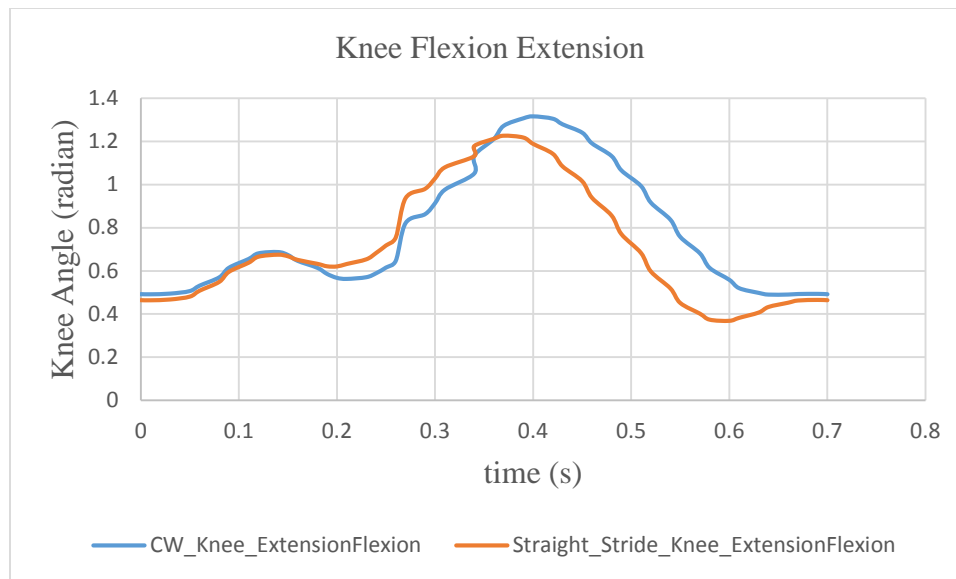
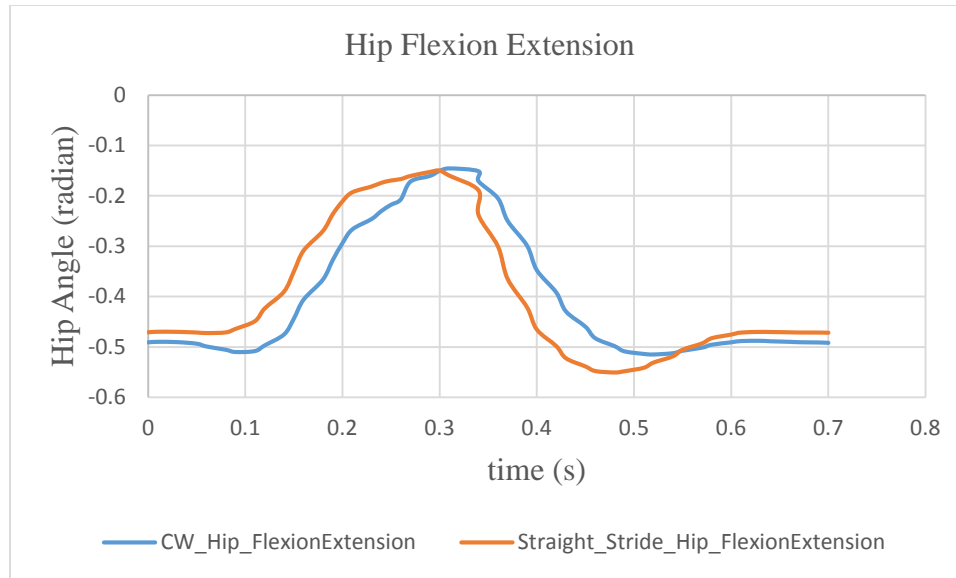


Figure 5.8: Comparison of Joint Torque Profiles for Straight Jogging Stride and Clock-wise Jogging Stride Simulations

5.1.2.4 Cause and Effect Studies

In this section, simulation results for different loading conditions are presented for the CW jogging motion. Figure 5.9 depicts the hip and knee joint torques, figures 5.10, 5.11 and 5.12 show the ground reaction force results and figure 5.13 shows joint angle profiles for three cases: no load, jogging with a 40 lb backpack and jogging with an 80 lb backpack. The 80 lb backpack case has a larger peak torque than 40 lb or no load cases. The ground reaction forces justifiably increase with increasing loads. Significant load effect is observed on the vertical GRF. For the forward force, the 80 lb backpack shows a greater minimum force compared to the 40 lb backpack. For the lateral GRF, the 80 lb backpack shows a larger peak force than the 40 lb backpack. The hip and knee joint angles do not show much change since the jogging velocity and step length is not changed. However, there is increased spine bending due to the added external load which is reflected well in the simulation results.

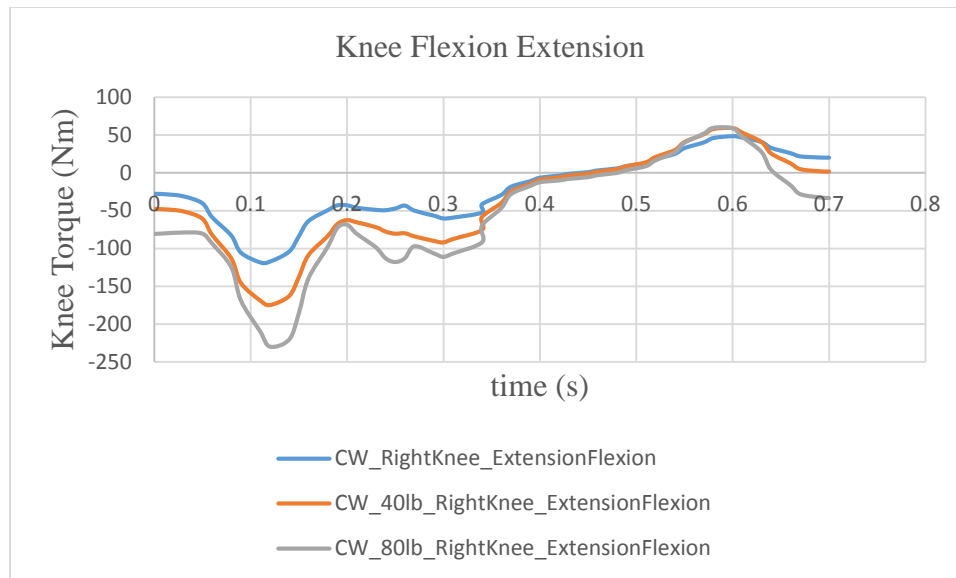
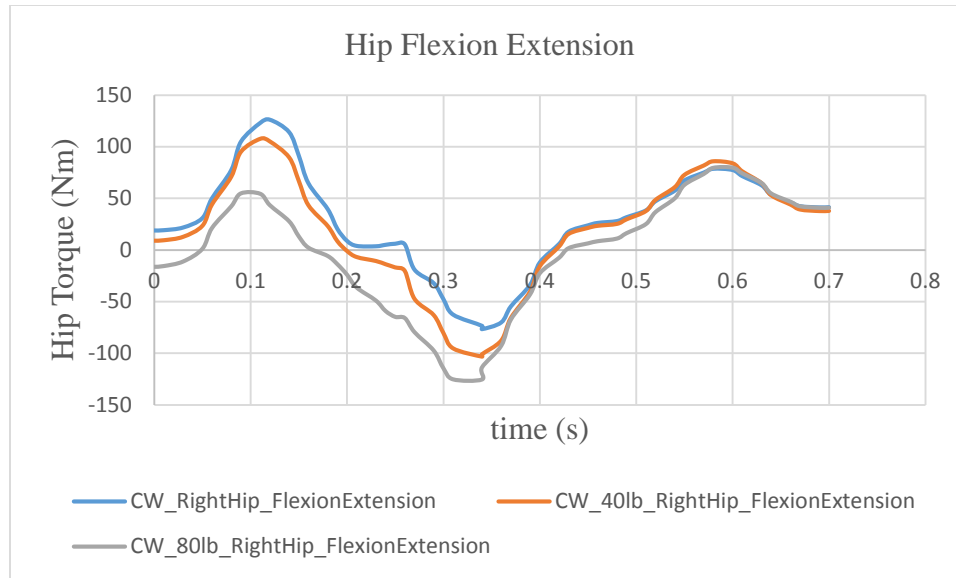


Figure 5.9: Comparison of Joint Torque Profiles for Clock-wise Jogging Stride Simulations with No Load, 40 lb Backpack and 80 lb Backpack

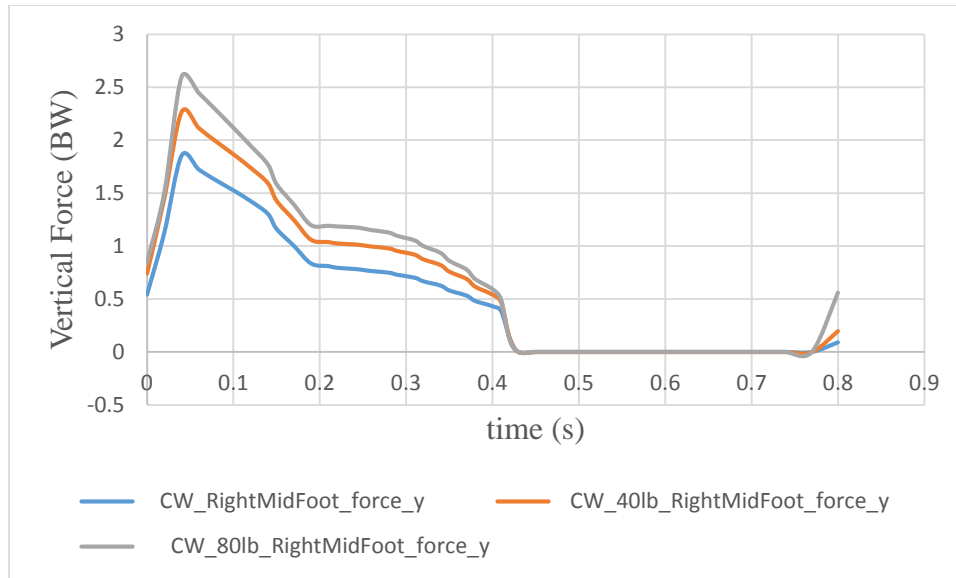


Figure 5.10: Comparison of Vertical GRF for Clock-wise Jogging Stride Simulations with No Load, 40 lb Backpack and 80 lb Backpack

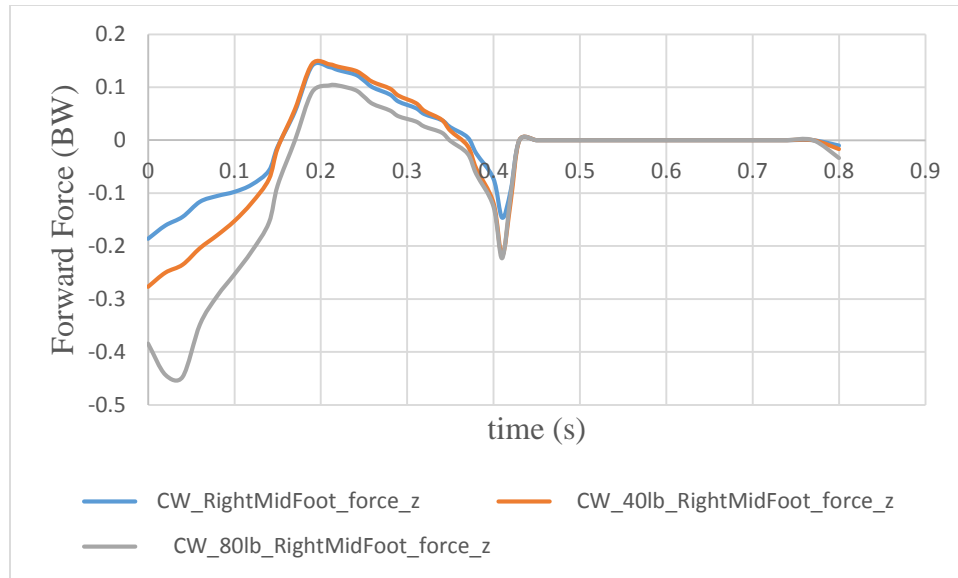


Figure 5.11: Comparison of Fore-Aft GRF for Clock-wise Jogging Stride Simulations with No Load, 40 lb Backpack and 80 lb Backpack

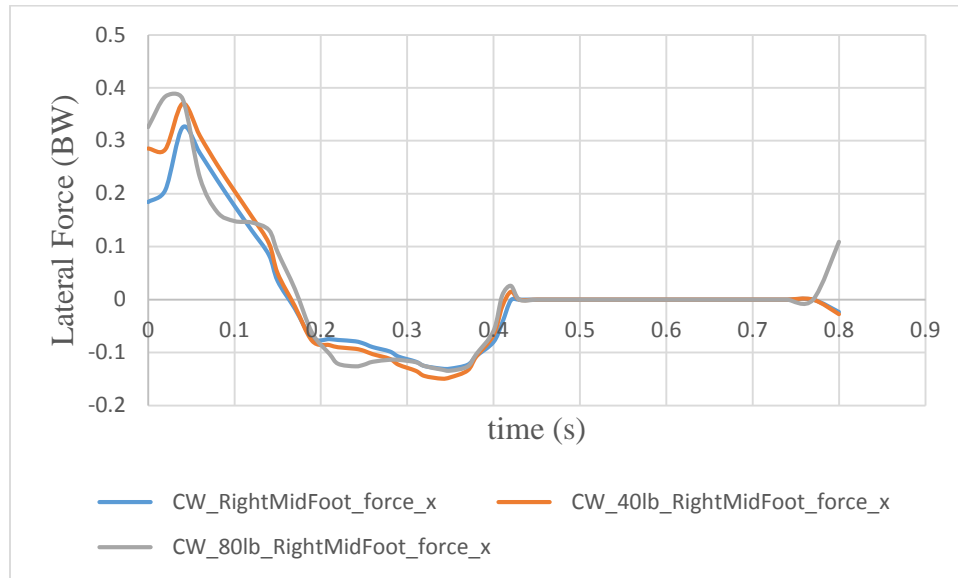
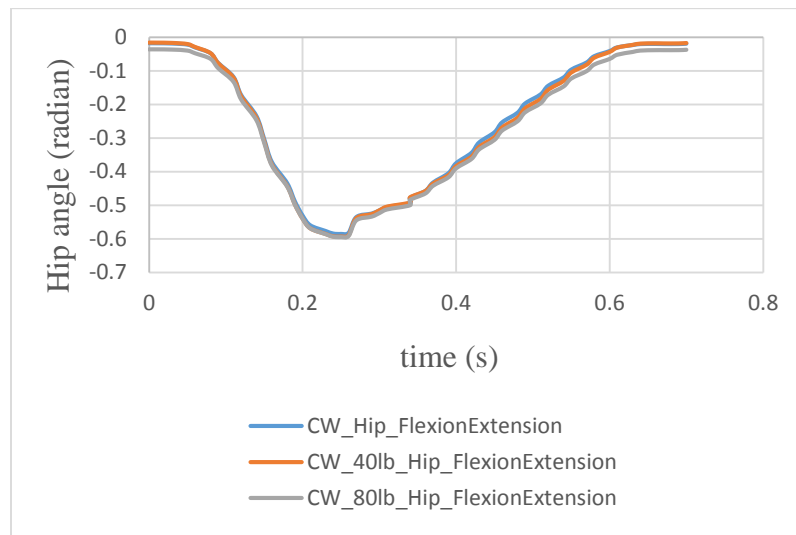


Figure 5.12: Comparison of Lateral GRF for Clock-wise Jogging Stride Simulations with No Load, 40 lb Backpack and 80 lb Backpack



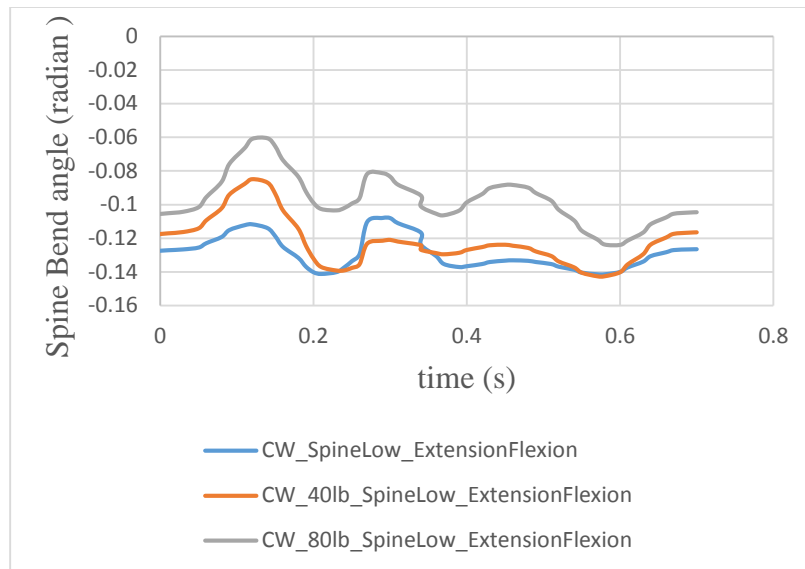
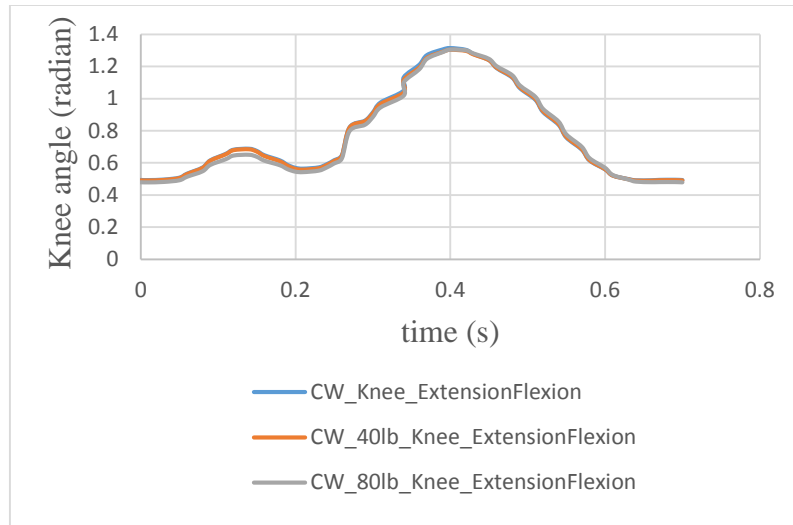


Figure 5.13: Comparison of Joint Angles for Clock-wise Jogging Stride Simulations with No Load, 40 lb Backpack and 80 lb Backpack

5.2 Counter Clock-wise Jogging

In this section, formulation and simulation results for counter clock-wise jogging along a curve are presented.

5.2.1 Optimization Formulation

5.2.1.1 Task Description

The task is described as follows: Given a marker, Santos jogs around the marker. The stride formulation is tested for this asymmetric task where motion of the left and right parts of the body is not the same and Santos carries a gun in his left hand.

5.2.1.2 Data Collection

A velocity of 2 m/s, an initial step length $L = 0.55$ m and a radius of curved path $R = 1.5$ m is used for the task. Step length L and curve radius R are used to calculate actual foot locations along the curve for the foot contact position constraint (Chung, 2009). The foot locations are calculated as described in section 5.1.1.2. Again, for the given values of step length L and radius R , the foot orientation angle θ is approximately 30 degrees and the distance covered in one stride is 1.6 m at a velocity of 2 m/s. The time duration for the stride is then calculated as $T = 1.6/2 = 0.8s$.

5.2.1.3 Optimization Design Variables

The joint angle profiles $\mathbf{q}(t)$ parameterized using B-spline approximation are used as design variables for the optimization problem.

5.2.1.4 Objective Function

Motion capture data has been used in this work to improve motion simulation. The difference or error between the desired joint angles from motion capture and the actual joint angles forms the first performance criterion. It is also termed as the tracking error and is minimized in the optimization formulation.

$$f_1 = \sum_{i=1}^{ndof} \int_{t=0}^T (q_{id}(t) - q_i(t))^2 dt \quad (5.12)$$

where $ndof$ is the number of DOF, q_{id} is the desired joint angle vector for the i th DOF and q_i is the actual joint angle vector for the i th DOF.

The time integral of the squares of all joint torques, also termed as dynamic effort, is used as the other performance criterion for the jogging motion (Fregly 2007, Xiang et al. 2010a):

$$f_2 = \sum_{i=1}^{ndof} \int_{t=0}^T \left(\frac{\tau_i}{|\tau|_{max}} \right)^2 dt \quad (5.13)$$

where $|\tau|_{max}$ is the maximum absolute value of all the joint torque limits; $ndof$ is the number of DOF; T is the last time point, i.e., total time.

The overall objective function is a weighted combination of the two performance measures stated above.

$$f(\mathbf{P}) = (w_1 * f_1) + (w_2 * f_2) \quad (5.14)$$

where w_1 and w_2 are the weights for the objective functions. Tracking error is minimized to get an initial kinematics solution with $w_1 = 1$ and $w_2 = 0$ which is used as the starting point when dynamic effort is added with $w_1 = 0.5$ and $w_2 = 0.5$. The weights for the objective functions are selected such that $\sum w_i = 1$.

5.2.1.5 Constraints

Two types of constraints are considered for the jogging optimization problem as specified before: time-dependent and time-independent constraints. The time-dependent constraints include (1) joint angle limits; (2) joint torque limits; and (3) ZMP stability. These constraints are detailed as follows:

(1) Joint angle limits

The physical range of motion of joints accounts for the joint angle limits (Xiang et al. 2010a).

$$\mathbf{q}^L \leq \mathbf{q}(t) \leq \mathbf{q}^U, \quad 0 \leq t \leq T \quad (5.15)$$

(2) Joint torque limits

The dynamic physical strength of joints accounts for the joint torque limits where the maximum strength (τ_i^L or τ_i^U) of a particular joint, i , of a person changes with a change in its joint angle position $q(t)$ and velocity $\dot{q}(t)$.

$$\tau_i(q(t), \dot{q}(t))^L \leq \tau_i(t) \leq \tau_i(q(t), \dot{q}(t))^U; \quad 0 \leq t \leq T; \quad i = 1, \dots, ndof \quad (5.16)$$

(3) ZMP stability

The stability condition is imposed by locating ZMP position in the foot supporting region (FSR) as follows (Xiang et al. 2010a):

$$z_{ZMP}(t) \in FSR, \quad y_{ZMP}(t) \in FSR, \quad 0 \leq t \leq T \quad (5.17)$$

Time independent constraints are as follows:

(1) Foot contacting positions

Foot contacting positions during the motion are specified based on the step length L to satisfy the step length constraint. The optimization process determines the initial and final postures, velocities and accelerations.

(2) Continuity conditions

$$\begin{aligned} q_i(0) - q_i(T) &= 0, & i &= 2, 3, \dots, n \\ \dot{q}_j(0) - \dot{q}_j(T) &= 0, & j &= 1, 2, \dots, n \\ |\ddot{q}_k(0) - \ddot{q}_k(T)| &\leq \varepsilon, & k &= 1, 2, \dots, n \end{aligned} \quad (5.18)$$

where n is the number of DOFs and ε is a positive number ranging from 0.001 to 10. The position continuity constraint is excluded for the first DOF which corresponds to global translation along the jogging direction. The continuity condition file is shown in Table 4.1 where 0 refers to no symmetry, 1 refers to continuity and -1 refers to symmetry. In some cases, a smaller value for ε for the acceleration continuity constraint may result in an infeasible solution indicating a conflict with other constraints. Hence, a large value for ε may be used for the constraint to account for the discontinuities resulting due to the impulse-like forces at toe-strike.

5.2.2 Results

The nonlinear optimization problem of counter clock-wise (CCW) jogging motion simulation with one-stride formulation is solved using a sequential quadratic programming (SQP) algorithm in SNOPT (Gill, Murray, and Saunders 2002). In addition to normal CCW jogging, cause and effect studies are presented for different loading conditions (40lb and 80 lb).

The optimization problem has 495 design variables (55 DOFs each with 9 control points) along with 1929 nonlinear constraints. Tracking error is minimized to get an initial kinematics solution which is used as the starting point when the other objective function of dynamic effort is added to solve the problem. The optimality and feasibility tolerances are both set to $\epsilon = 10^{-3}$ and the optimal solution is obtained in 1434 CPU seconds on an Intel i7, 16 GHz computer. Objective function values are 2.604 for tracking and 1.784 for dynamic effort objective. The results are compared with running simulation results from Chung (2009), other experiment results from literature (Novacheck, 1998) and the one-stride straight jogging simulation of Santos presented in chapter 4. Figure 5.14 shows slices of the motion at 0, 25, 50, 75 and 100 % of total time of motion.

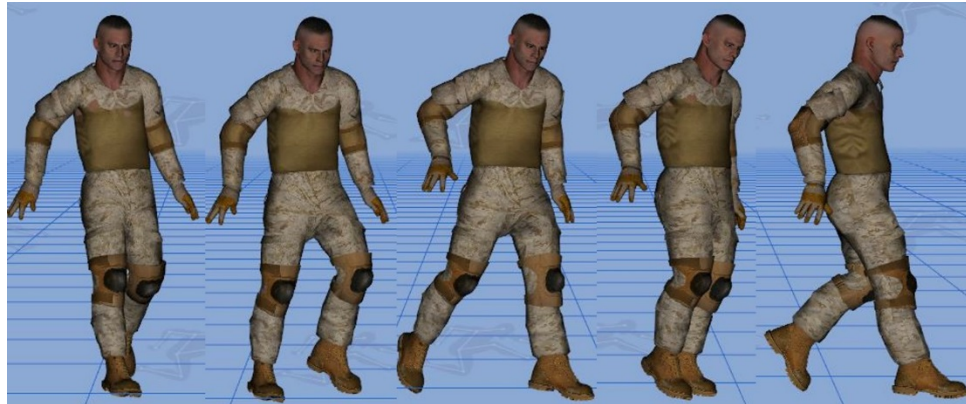


Figure 5.14: CCW Jogging Stride Motion Slices at 0, 25, 50, 75 and 100% T

5.2.2.1 Joint Torque Profiles

Figure 5.15 shows the joint torque profiles of hip and knee for the one-stride simulation of CW jogging on a curved path. The results compare well with running results of Chung (2009) and Novacheck (1998) and the straight stride results and show reasonable trend in general. The hip begins to flex with the left toe strike and maximum extension torque is reached with the right foot toe strike. The knee is flexed at the start when left toe strikes but then reverses to an extension torque.

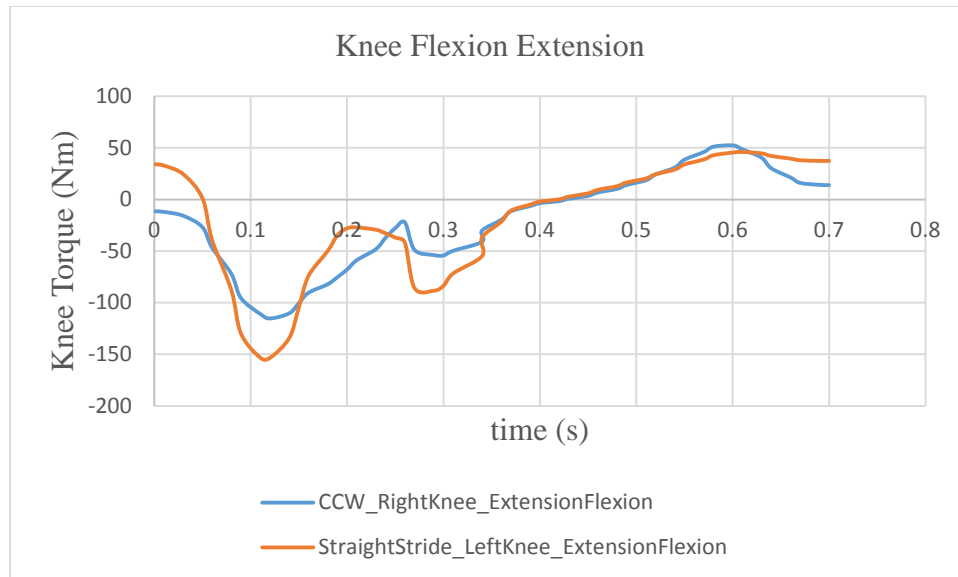
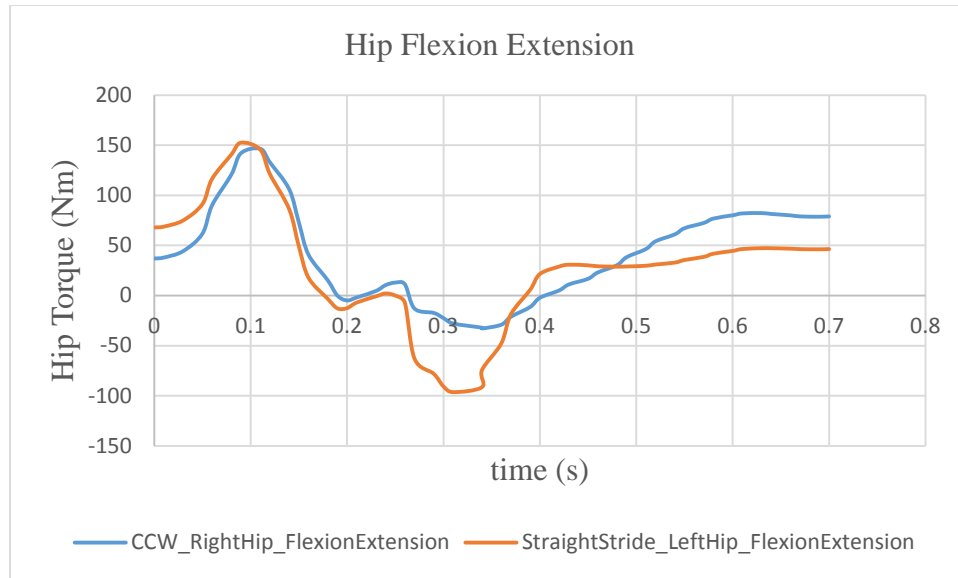


Figure 5.15: Comparison of Joint Torque Profiles for Straight Jogging Stride and Counter Clock-wise Jogging Stride Simulations

5.2.2.2 Ground Reaction Forces

Vertical ground reaction force (corresponding to the global y-axis) results are shown in figure 5.16. All GRFs are normalized to body weight (816.78 N). The results show a reasonable trend with the straight stride results and walking results. The peak force is well within the range reported by Keller (1996). Vertical force for CCW is comparable to straight jogging which is in contrast to the CW results and needs to be investigated further. Figure 5.17 depicts the forward GRF (corresponding to the global z-axis) and figure 5.18 shows the lateral GRF (corresponding to the global x-axis). The forward GRF compares well with Chung (2009) and Xiang (2008) as well as the straight stride results. The lateral/ medial force compares well with Chung (2009) and the straight stride results and provides the required centripetal force for the counter clock-wise jog.

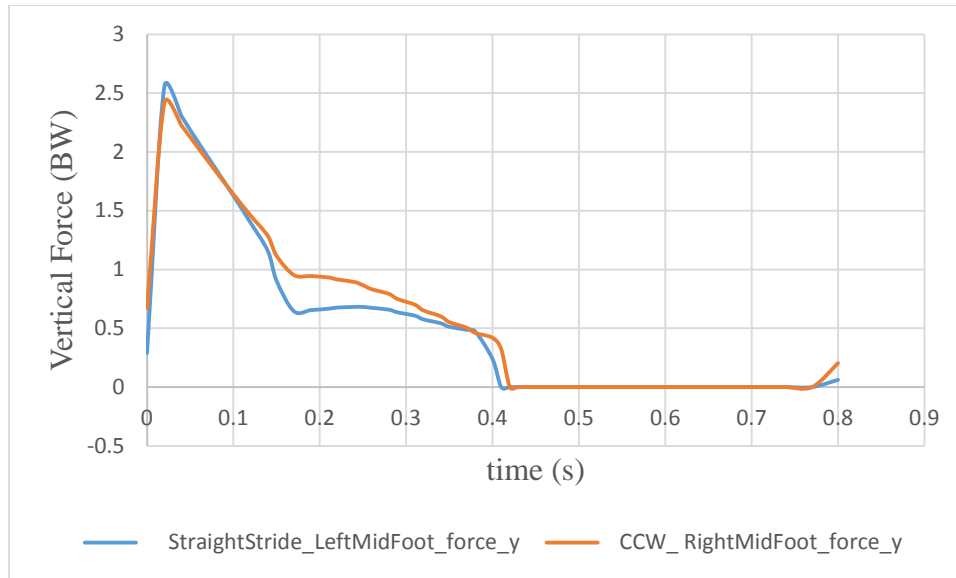


Figure 5.16: Comparison of Vertical GRF for Straight Jogging Stride and Counter Clock-wise Jogging Stride Simulations

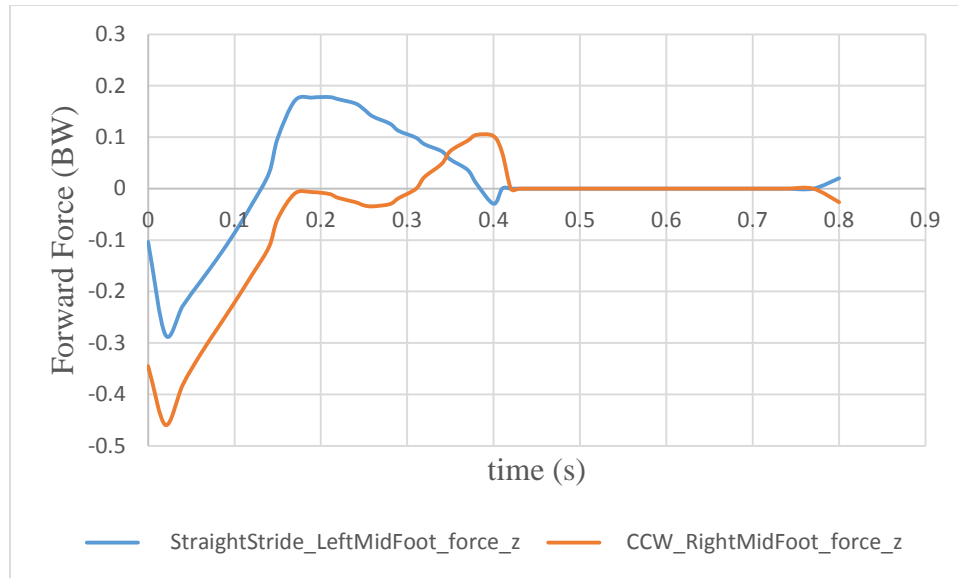


Figure 5.17: Comparison of Fore-Aft GRF for Straight Jogging Stride and Counter Clock-wise Jogging Stride Simulations

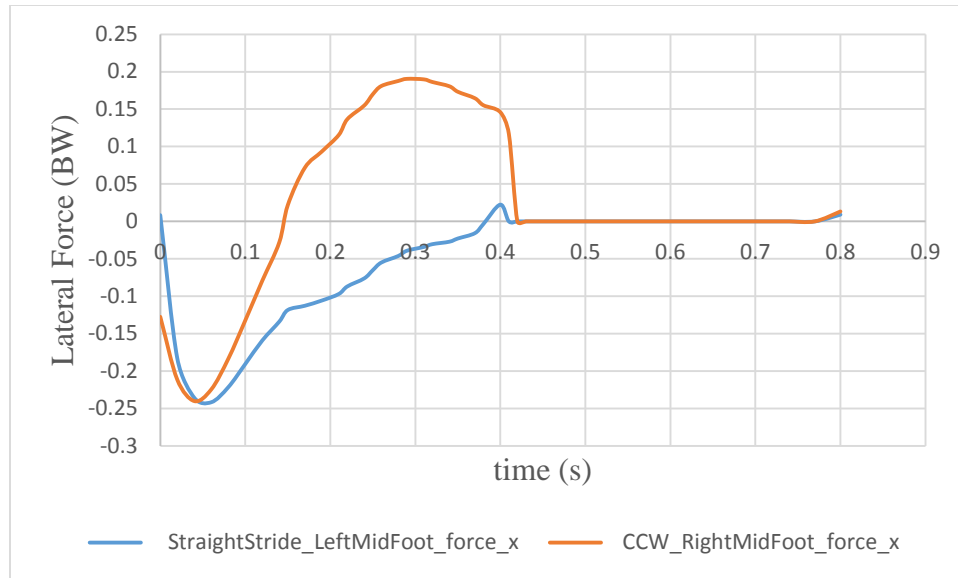


Figure 5.18: Comparison of Lateral GRF for Straight Jogging Stride and Counter Clock-wise Jogging Stride Simulations

5.2.2.3 Kinematics

Figure 5.19 depicts the hip and knee flexion and extension angles in radians. The results compare well with the literature (Novacheck, 1998) and show reasonable trend in general. The hip and knee joint angles compare well with the jogging one stride simulation hip and knee angles as well.

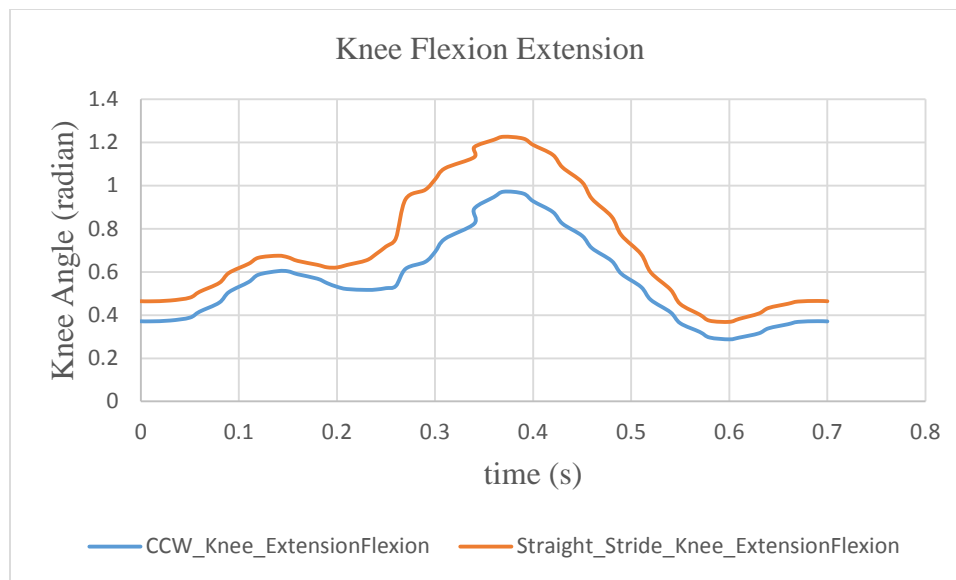
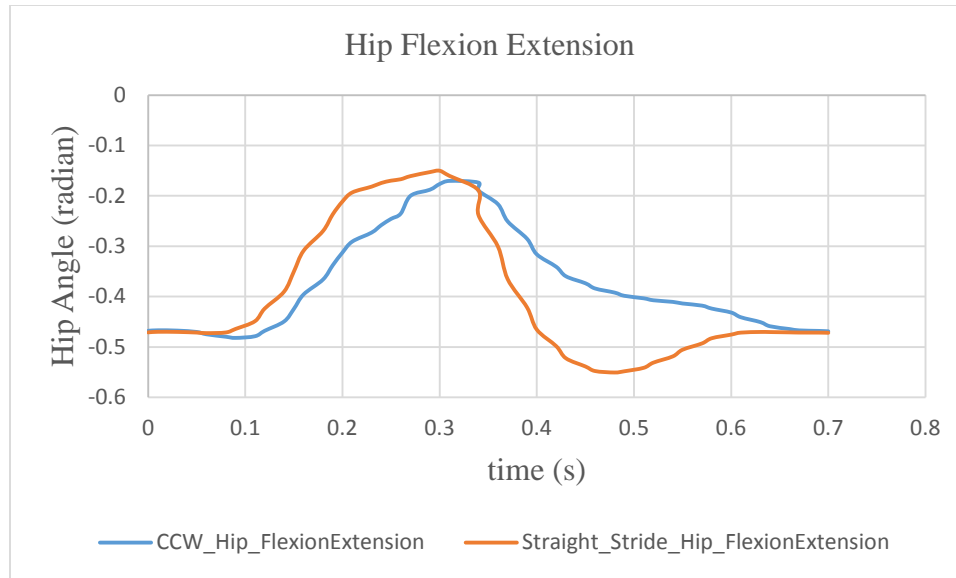


Figure 5.19: Comparison of Joint Angles for Straight Jogging Stride and Counter Clock-wise Jogging Stride Simulations

5.2.2.4 Cause and Effect Studies

In this section, simulation results for different loading conditions are presented for the CCW jogging motion. Figure 5.30 depicts the hip and knee joint torques, figures 5.21, 5.22 and 5.23 show the ground reaction force results and figure 5.24 shows joint angle profiles for three cases: no load, jogging with a 40 lb backpack and jogging with an 80 lb backpack. The 80 lb backpack case has a larger peak torque than 40 lb or no load cases. The ground reaction forces justifiably increase with increasing loads. Significant load effect is observed on the vertical GRF. For the forward force, the 80 lb backpack shows a greater minimum force compared to the 40 lb backpack. For the lateral GRF, the 80 lb backpack shows a larger peak force than the 40 lb backpack. The hip and knee joint angles do not show much change since the jogging velocity and step length is not changed. However, there is increased spine bending due to the added external load which is reflected well in the simulation results.

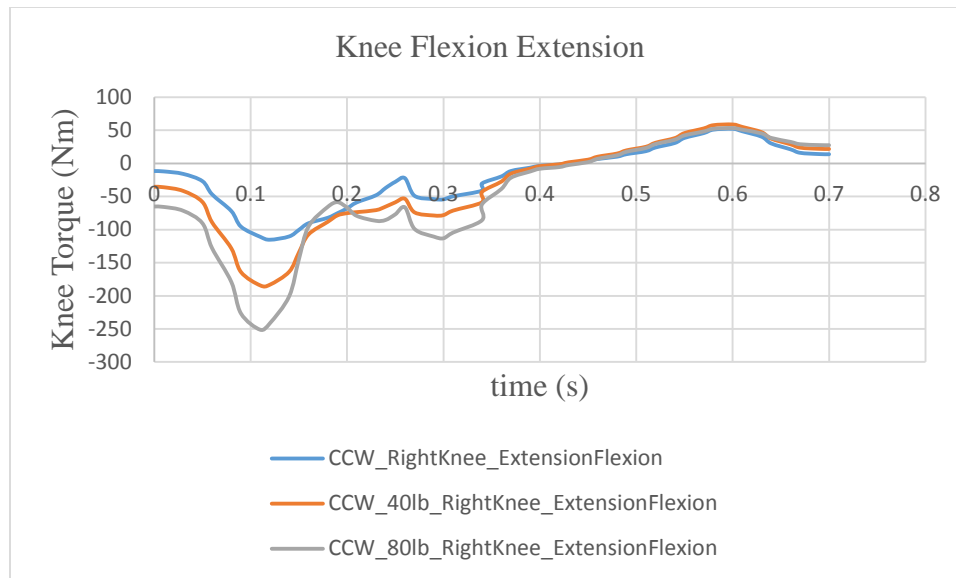
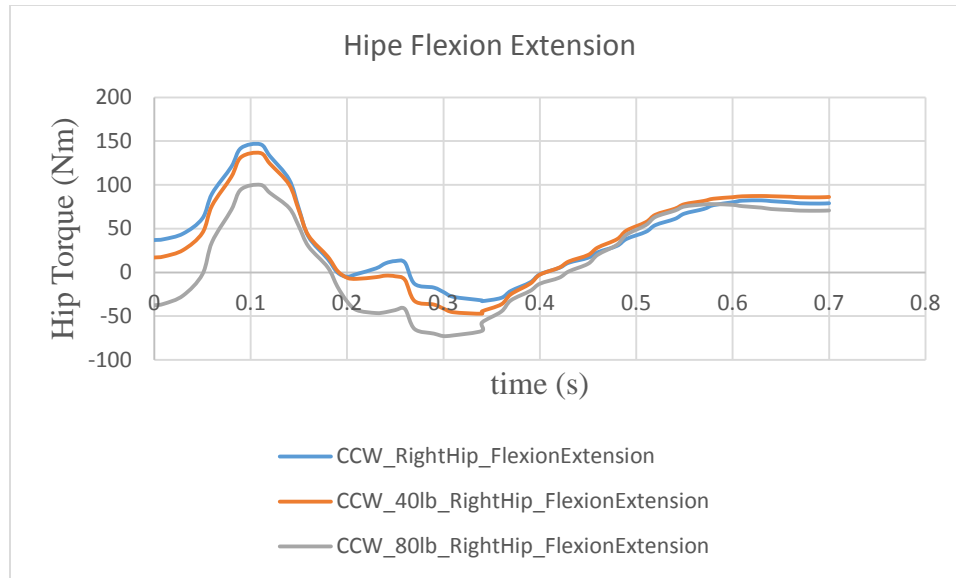


Figure 5.20: Comparison of Joint Torque Profiles for Counter Clock-wise Jogging Stride
 Simulations with No Load, 40 lb Backpack and 80 lb Backpack

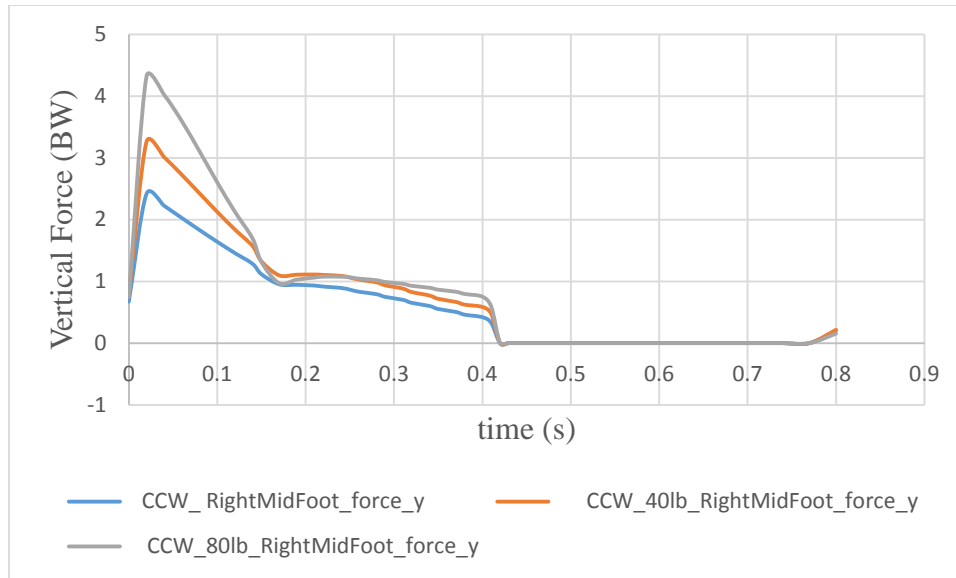


Figure 5.21: Comparison of Vertical GRF for Counter Clock-wise Jogging Stride

Simulations with No Load, 40 lb Backpack and 80 lb Backpack

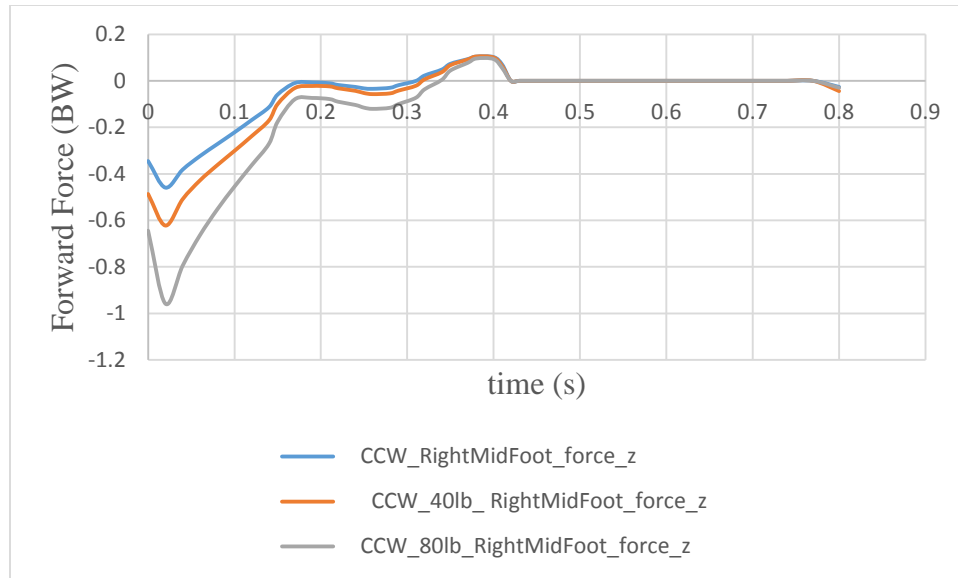


Figure 5.22: Comparison of Fore-Aft GRF for Counter Clock-wise Jogging Stride
 Simulations with No Load, 40 lb Backpack and 80 lb Backpack

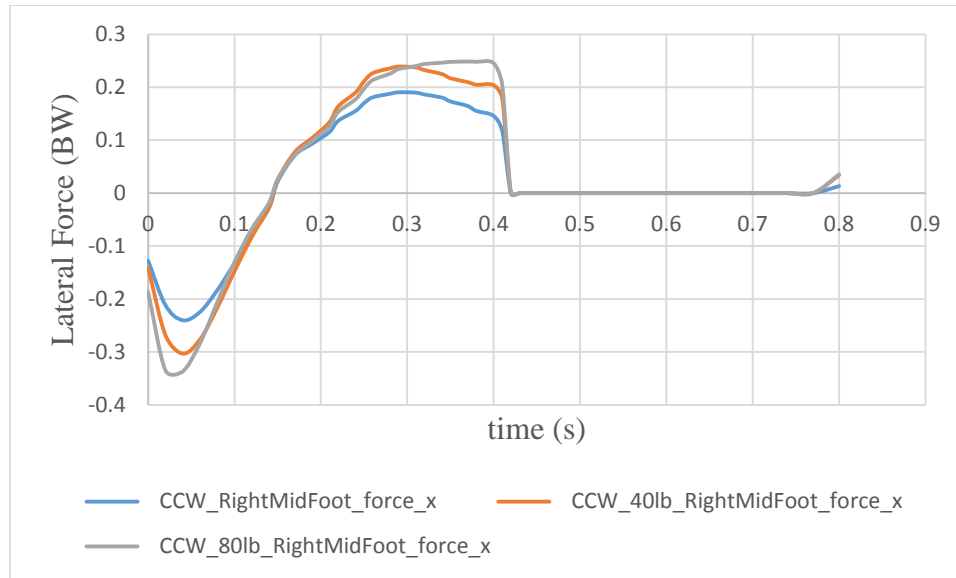
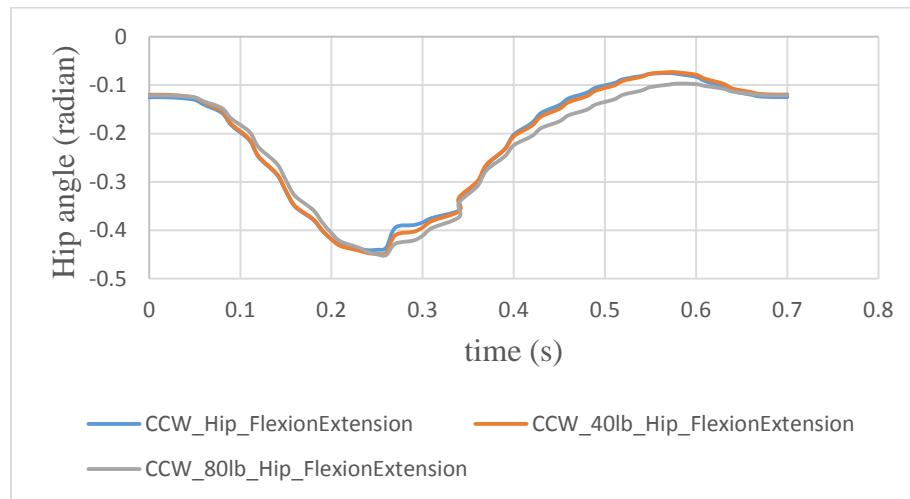


Figure 5.23: Comparison of Lateral GRF for Counter Clock-wise Jogging Stride Simulations with No Load, 40 lb Backpack and 80 lb Backpack



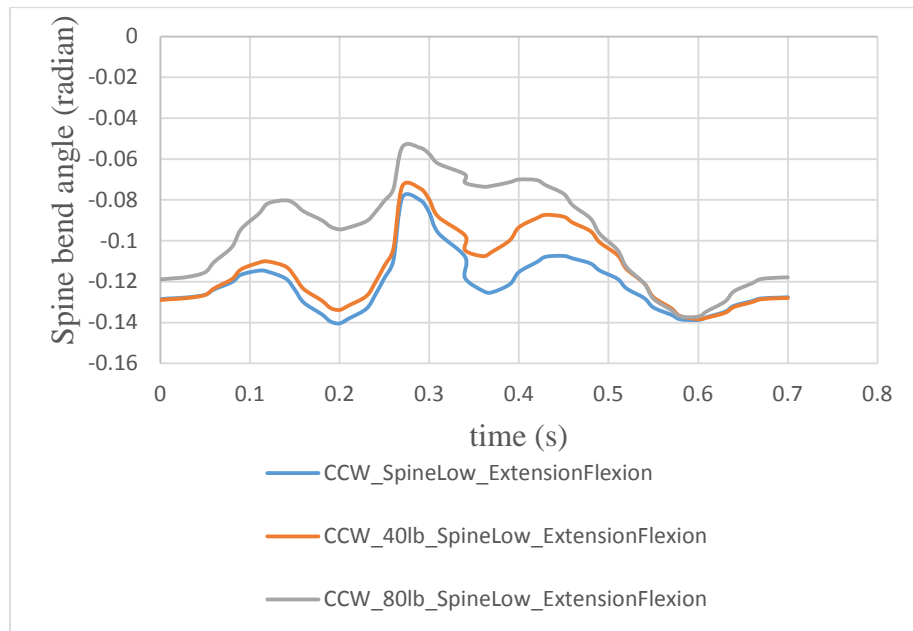
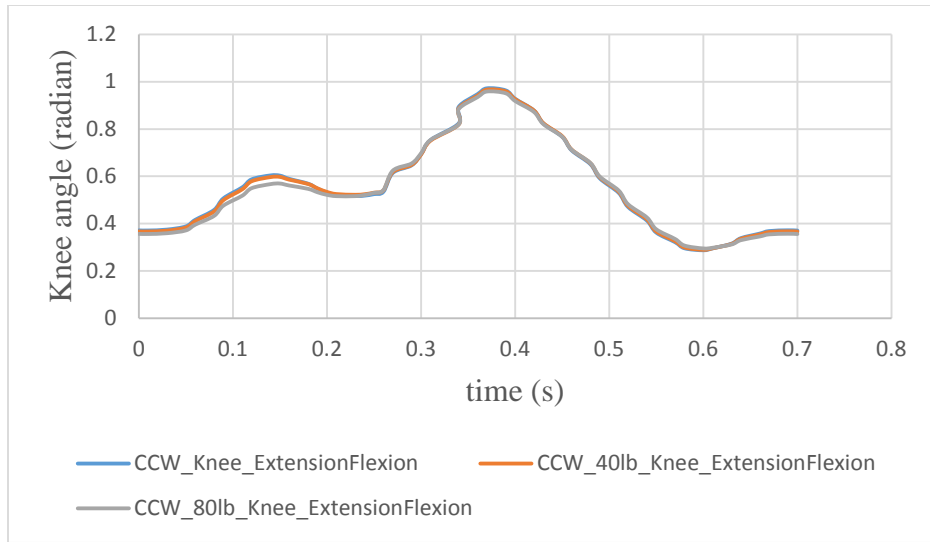


Figure 5.24: Comparison of Joint Angles for Counter Clock-wise Jogging Stride
 Simulations with No Load, 40 lb Backpack and 80 lb Backpack

CHAPTER 6: DISCUSSION, CONCLUSIONS AND FUTURE RESEARCH

6.1 Discussion

This work is aimed at bridging the gap in literature due to the lack of research work in three main areas: (1) simulations and experiments on running at speeds lower than 3 m/s, (2) Kinetics of fore-foot strike pattern in jogging and running and (3) the existence of a double support phase in running at slower speeds and its effects.

The results presented in this work provide some insights into the human jogging motion from a biomechanical perspective. A lowering of center of mass and increased spine flexion is observed as the motion changes from walking to jogging. The knee flexion is increased during the swing phase in jogging as compared to walking. There is increased hip adduction relative to the pelvis as a shock absorbing mechanism. The pelvis moves down during the stance phase and reverses motion during swing phase to create foot clearance. The hip and knee torques are increased during the swing phase for jogging. The ground reaction forces see a similar increase with increased velocity.

The results obtained by running the walking simulation with an increased velocity provided an unnatural walking motion. These results along with the visual results of the jogging simulation prove the hypothesis that simulation of human jogging by formulating the motion as a separate problem with different gait cycle phases and foot striking patterns as compared to walking provides more realistic motion. The jogging simulation results also show the cause and effect of external loading successfully, thus validating the robustness and practical application of predictive dynamics to digital human modeling.

A few challenges were associated with the formulation and implementation of the jogging task. The step formulation required changes to the code to incorporate the continuity constraint as it involved solving two optimization problems to obtain one entire stride. An additional objective function for the position symmetry had to be added to the step formulation for a smooth motion especially with external loading. Any changes to anthropometry or input velocity change the step length which correspondingly change the foot contact locations. Hence, modifications were made to the code to input foot contact locations from user interface based on the velocity and corresponding step length. Curved jogging uses a stride formulation assuming the starting posture entering the curve is the same as the end posture into the curve. A different optimization problem could be used for the motion entering the curve as compared to the motion during the curve to get a more realistic motion and needs to be investigated further.

Results obtained from jogging simulations such as this current work and experimental studies have many applications. Kinetics obtained from jogging simulations can be used to assess strength requirements for internal and external prostheses (Paul, 1999). It can also be used to assist rehabilitation teams when considering returning individuals back to activity following lower-limb surgical procedures, for preventing overuse injury and to provide exercise recommendations for people at greater risk of exacerbating chronic joint pain (Kaplan et.al, 2013). Another major application of understanding jogging kinematics and kinetics is in monitoring the dynamics of subjects suffering from various diseases such as Multiple Sclerosis (MS) and detecting the mobility limitations associated with such diseases. Kalron (2013) explained the limitations of

current tests used to quantify and assess disability and showed the importance of adding more demanding tests such as jogging tasks to improve gait evaluation.

6.2 Conclusions

Optimization-based dynamic simulation of human jogging motion has been presented in this work. The jogging problem is formulated using the predictive dynamics methodology. The nonlinear optimization problem is solved using an algorithm based on the sequential quadratic programming approach. Santos, a 55 DOF digital human, developed at the Virtual Soldier Research (VSR) lab at the University of Iowa, is used as the human model for this work. Denavit-Hartenberg method is used for kinematics analysis. B-spline interpolation method is used to discretize the time domain. The control points for the joint angle profiles are treated as the design variables in this representation. Two formulations are presented for the simulation of jogging motion with fore-foot strike pattern and a reduced double-support phase compared to walking. One-step formulation is presented for jogging on a straight path and one-stride formulation is presented for jogging on a straight path as well as for clock-wise and counter clock-wise jogging on a curved path. Error in tracking motion capture data, dynamic effort and error in maintaining symmetry at the position level are used as performance measure for the step formulation and error in tracking motion capture data and dynamic effort are used as performance measures for the stride formulation. The joint angle profiles, joint torque profiles and ground reaction forces are determined. Cause and effect studies are presented for different backpack loading conditions and reasonable responses are achieved which shows that the presented formulations are quite robust and predict natural human jogging motion.

6.2 Future Work

There exist a few issues pertaining to the current work as well as the motion simulation framework in general which should be investigated further. In general, multiple objectives govern the human motion. Therefore, other performance measures such as fatigue and discomfort need to be investigated. Better motion capture data can be obtained to make simulations of human motion even more realistic. Results presented in this work need to be validated and investigated further. The step formulation should be applied to jogging on a curved path to provide more flexibility. Other formulations and discretization strategies need to be investigated to improve the numerical performance of the optimization problem. Additional jogging velocities and varying anthropometries should be tested. Asymmetric loading and restricted range of motion cases should be studied with the presented formulations for further validation.

REFERENCES

- Bruderlin, A. and Calvert, T. 1996. "Knowledge-driven, interactive animation of human running." Proceedings of the Conference on Graphics Interface, 213-221.
- Burgess, DJ, Naughton, G, and Norton, KI. Profile of movement demands of national football players in Australia. *J Sci Med Sport* 9: 334–341, 2006.
- Castro, A., LaRoche, D. P., Fraga, C. H. W., Gonsalves, M. (2013), 'Relationship between running intensity, muscle activation, and stride kinematics during an incremental protocol', 28 (4), pp e85-e92, (2013). Cavanagh PR, Lafortune MA. Ground reaction forces in distance running. *J Biomech* 1980; 13: 397-406
- Cavanagh, P.R., Williams, K.R. & Clarke, T.E. (1981). A comparison of ground reaction forces during walking barefoot and in shoes. IN: A. Morecki, K., Kedzior, & A. Wit (Eds.): *Biomechanics VII* (pp. 15 1-156). Baltimore: University Press.
- Celik, Huseyin, and Stephen J. Piazza. 2013. "Simulation of Aperiodic Bipedal Sprinting." *Journal of Biomechanical Engineering* 135 (8): 081008–081008. doi:10.1115/1.4024577.
- Chevallereau, C., and Aousin, Y. (2001), "Optimal Reference Trajectories for Walking and Running of a Biped Robot," *Robotica*, 19, 557–569.
- Chung, Hyun-Joon. "Optimization-based dynamic prediction of 3D human running." PhD (Doctor of Philosophy) thesis, University of Iowa, 2009.
- Cross R. (1998) Standing, walking, running and jumping on a force plate. *American Journal of Physics* 67(4), 304-309
- D.B. Dwyer, T.J. Gabbett, Global Positioning System data analysis: velocity ranges and a new definition of sprinting for field sport athletes, *J Strength Cond Res*, 26 (3) (2012), p. 818
- De Boor, C. 2001. *A Practical Guide to Splines*. revised edition. New York: Springer.
- Demura, T., Demura, S. I. and Shin, S. (2010), 'Comparison of gait properties during level walking and stair ascent and descent with varying loads'. *Health*, 2(12): 1372-6
- Denavit, J. and Hartenberg, R. S. 1955. "A kinematic notation for lower-pair mechanisms based on matrices." *ASME Journal of Applied Mechanics*, 22, 215–221.
- Dog̃ramacı, SN and Watsford, ML. A comparison of two different methods for time-motion analysis in team sports. *Int J Perform Anal Sport* 6: 73–83, 2006.
- Finch, A. (1995) "Alterations in ground reaction forces during tethered walking".

Frederick EC, Hagy JL, Mann RA. The prediction of vertical impact force during running. J Biomech 1981; 14: 498

Fregly, B.J., Reinbolt, J.A., Rooney, K.L., Mitchell, K.H., Chmielewski, T.L., 2007. Design of patient-specific gait modifications for knee osteoarthritis rehabilitation. IEEE Transactions on Biomedical Engineering, 54(9), 1687-1695.

Gazendam, M. G. and Hof, A. L. (2007), Averaged EMG profiles in jogging and running at different speeds. Gait Posture 25, 604-614.

Gill, P.E., Murray, W., Saunders, M.A. (1997): SNOPT: An algorithm for large-scale constrained optimization. Report NA97-2, University of California, San Diego

Hamill, J., B.T. Bates, KM. Knutzen and J.A. Sawhill, 1983. Variations in ground reaction force parameters at different running speeds. Human Movement Science 2, 47-56.

Harman E , Han K-H , Frykman P . Load-Speed interaction effects on the biomechanics of backpack load carriage . RTO Human Factors and Medicine Panel . 2000 ; 5 : 1 – 16 .

Hart, J.M., Fritz, J.M., Kerrigan, D.C., Ingersoll, C.D., 2009a. Jogging kinematics following lumbar paraspinal muscle fatigue. J. Athl. Train. 44 (5), 475–481. Kalron A, Dvir Z, Givon U, Baransi H, Achiron A. Gait and jogging parameters in people with minimally impaired multiple sclerosis. Gait Posture. 2013 Aug.

Hirai, K., Hirose, M., Haikawa, Y., and Takenaka, T. 1998. “The development of Honda humanoid robot.” Proceedings of the IEEE international Conference on Robotics and Automation, vol. 2, 1321-1326.

Hodgins, J. 1996. “Three-dimensional human running.” *Proceedings of the International Conference on Robotics and Automation*. vol. 4, 3271-3276.

J. Grizzle, J. Hurst, B. Morris, H.-W. Park, and K. Sreenath, “MABEL, a new robotic bipedal walker and runner,” in Proc. American Control Conf. , St. Louis, MO, June 2009, pp. 2030–2036.

J.P. Paul, Strength requirements for internal and external prostheses, Journal of Biomechanics, 32 (1999), pp. 381–393

Kaplan Y, Barak Y, Palmonovich E, Nyska M, Witvrouw E. Referent body weight values in over ground walking, over ground jogging, treadmill jogging, and elliptical exercise. Gait Posture. 2014;39:558–562.

Keller, T. S. et al. (1996) Relationship between vertical ground reaction force and speed during walking, slow jogging, and running. Clin. Biomech. 11, 253–259 (1996)

Kim, J., Abdel-Malek, K., Yang, J., Marler, T., “Prediction and Analyses of Human Motion Dynamics Performing Different Tasks”, International Journal of Human Factors Modelling and Simulation, Vol. 1, No. 1, (2006).

Kuntz, J. R., Terauds. J., (1983), 'Force measurements in jogging using biomechanics cinematography', International Symposium on Biomechanics in Sports (1983).

Lieberman D.E., Venkadesan M., Werbel W.A., Daoud A.I., D'andrea S., Davis I.S., Mang'eni R.O., Pitsiladis Y. (2010) Foot strike patterns and collision forces in habitually barefoot versus shod runners. *Nature* 463, 531-U149.

Munro CF, Miller DI, Fuglevand AJ. Ground reaction forces in running: a reexamination. *J Biomech* 1987; 20: 147-55

Nagasaka, K., Kuroki, Y., Suzuki, S., Itoh, Y. and Yamaguchi, J. 2004. "Integrated motion control for walking, jumping and running on a small bipedal entertainment robot." Proceedings of the IEEE International Conference on Robotics and Automation, vol. 4, 3189-3194.

Nigg BM, Bahlsen HA, Luethi SM, Stokes S. The influence of running velocity and midsole hardness on external impact forces in heel-toe running. *J Biomech* 1987; 20: 951-9

Novacheck, T. 1998. "Review paper: The biomechanics of running." *Gait and Posture*, 7, 77-95.

Öunpuu, S. 1994. "The biomechanics of walking and running." *Clinics in Sports Medicine*, 13(4), 843-863.

Raynor, Annette J; Yi, Chow Jia; Abernethy, Bruce; Jong, Quek Jin (2002). "Are transitions in human gait determined by mechanical, kinetic or energetic factors?", *Human Movement Science* 21 (5–6): 785–805.

Roussel L, Canudas-de-Wit C, Goswami A (1998) Generation of energy optimal complete gait cycles for biped robots. *Proc IEEE Int Conf Robotics Automation* 3:2036–20413.

Sasaki K, Neptune RR Differences in muscle function during walking and running at the same speed. *J Biomech*. 2006; 39(11): 2005–2013

Smoliga, J.M., Hegedus, E.J., Ford, K.R., Increased physiologic intensity during walking and running on a non-motorized, curved treadmill, *Physical Therapy in Sport* (2014), doi: 10.1016/j.ptsp.2014.09.001.

T. Lens, K. Radkhah, and O. von Stryk, "Simulation of dynamics and realistic contact forces for manipulators and legged robots with high joint elasticity," in *Int. Conf. on Advanced Robotics*, pp. 34–41, 2011.

Xiang, Y. (2008). "Optimization-based dynamic human walking prediction," PhD diss University of Iowa.

Xiang Y, Chung HJ, Kim JH, Bhatt R, Rahmatalla S, Yang J, Marler T, Arora JS, Abdel-Malek K. (2010a) Predictive dynamics: an optimization-based novel approach for human motion simulation. Struct Multidisc Optim.

Xiang, Y., Arora J.S., Chung, H.J., Kwon, H.J., Rahmatalla, S., Bhatt, R., Abdel-Malek, K., (2012a) Predictive simulation of human walking transitions using an optimization formulation. Structural and Multidisciplinary Optimization, 45(5), 759-772.